Ch. 5: Conductivity, Modulus & Dielectric Analysis

****

This chapter deals with various formalisms including impedance, frequency independent bulk (dc) conductivity, frequency dependent (ac) conductivity, relaxation and dielectric properties of the as prepared polymeric blend specimens. The influence of concentrations of various constituents and temperature on all the above mentioned formalisms is discussed thoroughly in this chapter.

****

This chapter deals with thorough investigation of the electrical properties viz. impedance, conductivity, dielectric and relaxation properties of the as prepared Ag^+ and Li^+ conducting blend polymer electrolyte systems, discussed briefly as follows.

5.1 Ag^+ Conducting Blend Polymer Electrolyte Systems

5.1.1 *Impedance Studies*

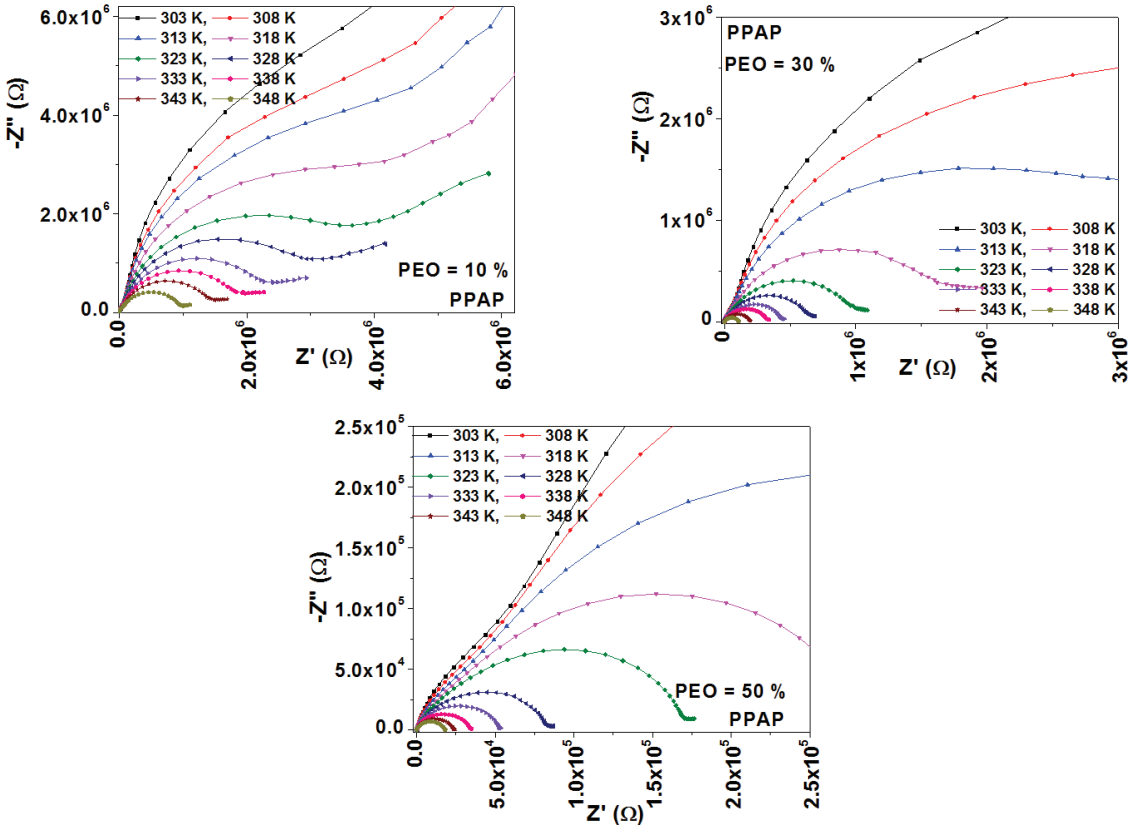

Fig. 5.1 (a) Nyquist plots of blend specimens of PPAP series at different temperatures

Nyquist (Complex Impedance) plots, plotted using complex impedance data, provide information regarding true bulk resistance of the specimen under test. Considering this, the Nyquist plots of blend specimens of PPAP ($[PVA_{(100-x)} : PEO_{(x)}]$ – 5 wt% $AgNO_3$ – 10 wt% PEG) series are recorded at different temperatures, plotted as shown in Fig. 5.1 (a) and investigated thoroughly to understand variation in their bulk resistance with respect to temperature ranging from 303 K to 348 K. Every Nyquist plot shows the presence of a

depressed semicircle at high frequency region at all temperatures, which occurs due to parallel combination of resistor (bulk resistance) and capacitor (bulk capacitance) of blend specimens thus, indicating their partially resistive and capacitive nature. This depressed semicircle is at times followed by an inclined spike/spur at low frequency side which is not only a characteristic feature and essential property of any ionic conductors and dielectric materials but also corresponds to electrode-electrolyte interface polarization effect [1-7]. Basically, appearance of spike in Nyquist plots is a signature of divergence from ideal behaviour [8,9]. Such a semicircle followed by a spike in Nyquist plots is an inherent property of elementary jump of ion owing to stored local energy [10]. As clearly visible from Fig. 5.1 (a) for blend specimens of PPAP series, intercept of real axis (Z') shifts gradually towards origin as temperature increases [11,12]. Such a phenomenon indicates gradual reduction in bulk resistance of the specimens as temperature rises from 303 K to 348 K.

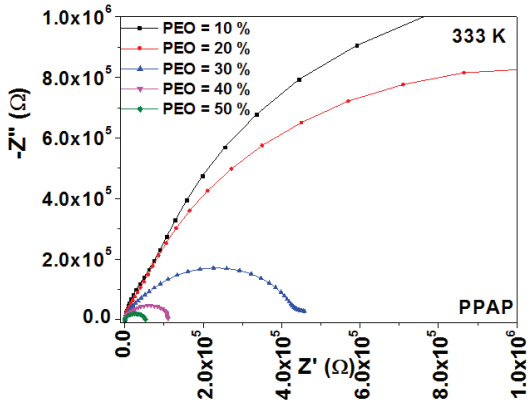

Fig. 5.1 (b) Nyquist plot of blends of PPAP series at various PEO concentrations at 333 K

Additionally, Nyquist plot as depicted in Fig. 5.1 (b) for blend specimens of PPAP series at each PEO concentration indicates the presence of a single semicircle. Intercept of real axis (Z') systematically shifts towards origin with substantial addition of PEO in blends, hence indicating gradual decrement in bulk resistance. As seen from Fig. 5.1 (b), the blend with highest concentration of PEO of 50 % depicts lowest bulk resistance.

On the other hand, the temperature-wise Nyquist plots of the blend specimens of PPAPA series given as '[$PVA_{(50)}$: $PEO_{(50)}$] – 5 wt% $AgNO_3$ – 10 % PEG – x wt% Al_2O_3', are depicted in the Fig. 5.2 (a). Likewise, observed for the blends of PPAP series, the Nyquist plots of blends of PPAPA series also show the presence of a single semicircle at high frequency side followed by a small spur at low frequency region. However, as temperature increases, the intercept of real axis (Z') systematically shifts towards origin, hence, indicating substantial reduction in bulk resistance of nano-composite blends.

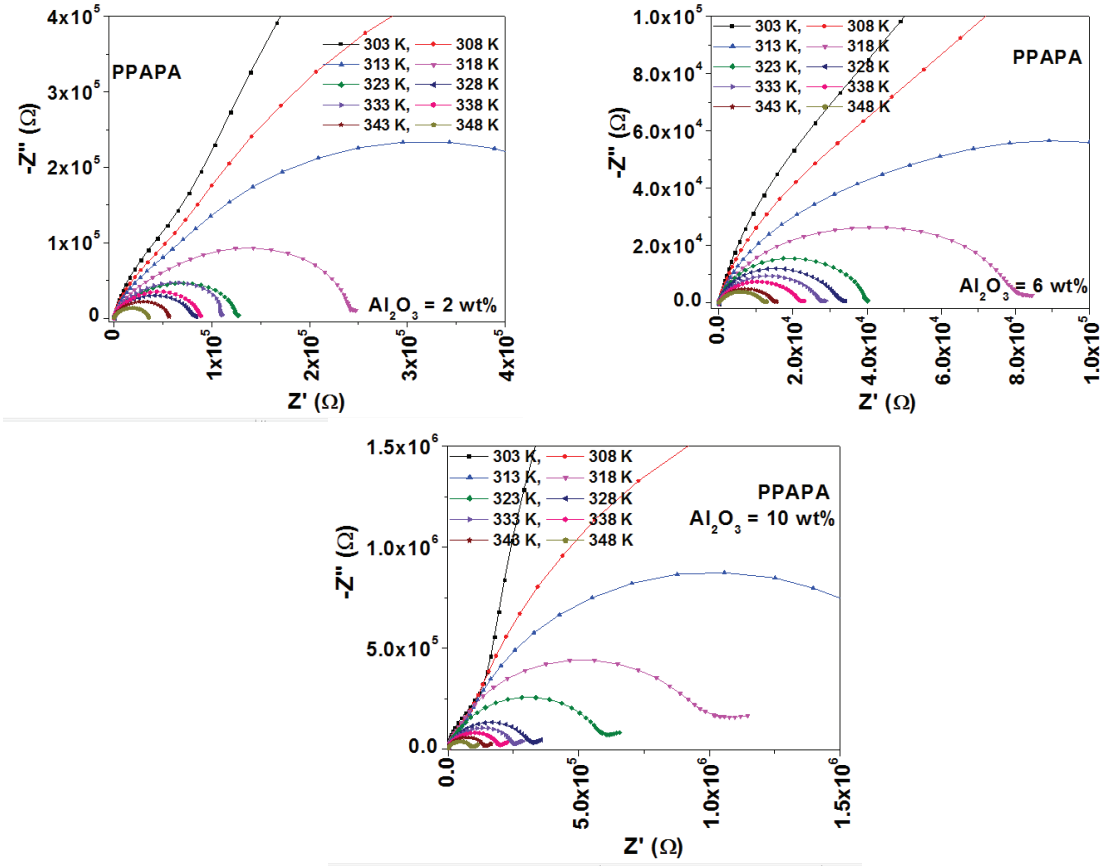

Fig. 5.2 (a) Nyquist plots of blend specimens of PPAPA series at different temperatures

Further, the Nyquist plot of the blends of PPAPA series plotted at different Al_2O_3 concentrations as depicted in Fig. 5.2 (b), shows a systematic shift of intercept of real axis (Z') of semicircles towards origin as content of Al_2O_3 increases in blends upto 6 wt%. This suggests a gradual reduction in bulk resistance of nano-composite blends with substantial

addition of Al_2O_3 therein. But with further addition of nano-filler in blends, this intercept shifts away from the origin hence, indicating increase in their bulk resistance.

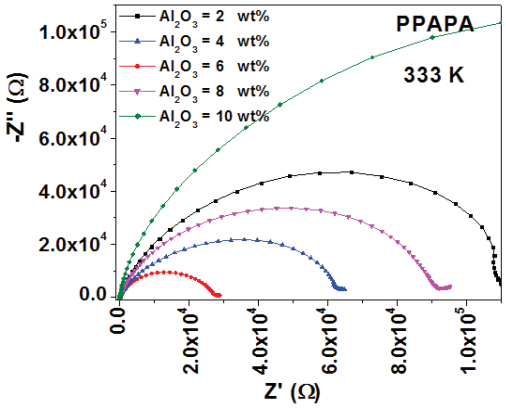

Fig. 5.2 (b) Nyquist plot of blends of PPAPA series at various Al_2O_3 concentrations at 333 K

5.1.2 *ac Conductivity Studies*

Using complex impedance data, ac conductivity spectra of blends of PPAP and PPAPA series are plotted at different temperatures and shown in respective Figs. 5.3 (a) and 5.4 (a). As observed from the figures, ac conductivity plot shows a frequency independent plateau at low frequency, usually attributed to dc conductivity. Such a frequency independent region corresponds to free charge carriers in conducting polymer electrolytes. But beyond a certain characteristic frequency, this frequency independent conductivity switches to frequency dependent conductivity hence, suggesting the beginning of relaxation phenomenon. This frequency dependent conductivity which increases with increasing frequency refers to ac conductivity and occurs when trapped charge carriers are activated and finally, released at appreciably high frequencies. As temperature increases, this hopping frequency gradually shifts towards the higher frequency side.

Interestingly, ac conductivity spectrum for blend specimen with 10 % of PEO of PPAP series as shown in Fig. 5.3 (a) shows presence of a double step-like feature corresponding to double relaxations in the entire temperature range. These double relaxations supposedly indicate the immiscibility of PVA and PEO host polymers and hence, correspond to their

individual phases in the blend matrices. But with further addition of PEO (> 20 %), single relaxation feature gradually dominates over double relaxation feature and become significantly prominent even at lower temperatures. Such a single relaxation feature is an indicative of the formation of a single homogenous PVA and PEO polymeric 'blend' phase. This discussion is also favoured by the Fig. 5.3 (b) wherein, ac conductivity data is plotted against logarithmic values of frequency at different PEO concentrations. Further, as seen from Fig. 5.3 (b), the dispersion frequency of ac conductivity curves shifts systematically towards higher frequency side with substantial increment of PEO in PVA-PEO blends.

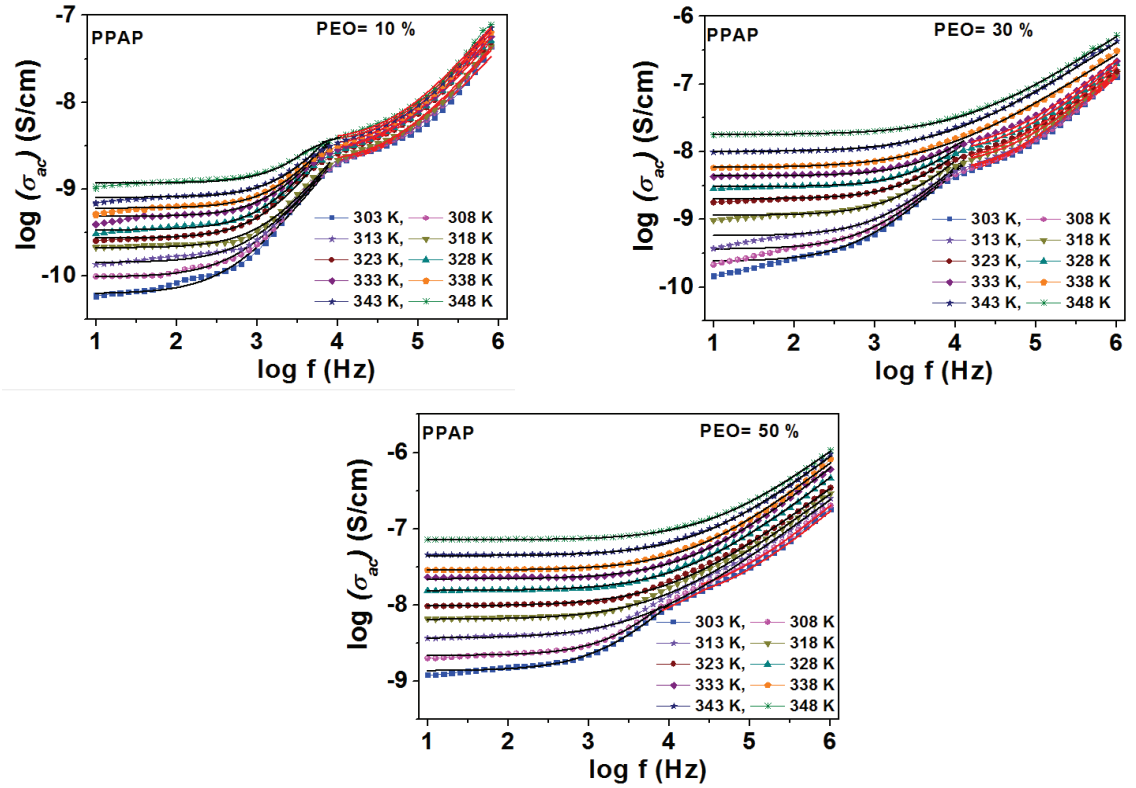

Fig. 5.3 (a) ac conductivity plots of blend specimens of PPAP series at different temperatures

Further, upon incorporation of various amounts of the Al_2O_3 nano-filler from 2 wt% to 10 wt% in the blends, this double relaxation feature is still observed in the respective ac conductivity spectrum as seen from Fig. 5.4 (a), but only at lower temperatures of 303 K to 313 K. However, at temperatures higher than 313 K, PEO chains may be reorganizing,

resulting in the uniform miscibility of the blend. Such an arrangement forms a single PVA-PEO blend phase which becomes significantly prominent at high temperatures.

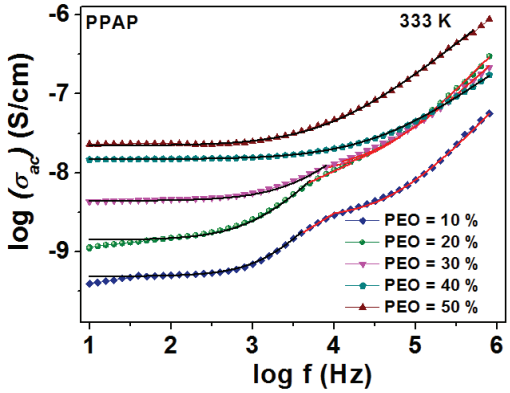

Fig. 5.3 (b) ac conductivity spectrum of blends of PPAP series at different PEO concentrations at 333 K

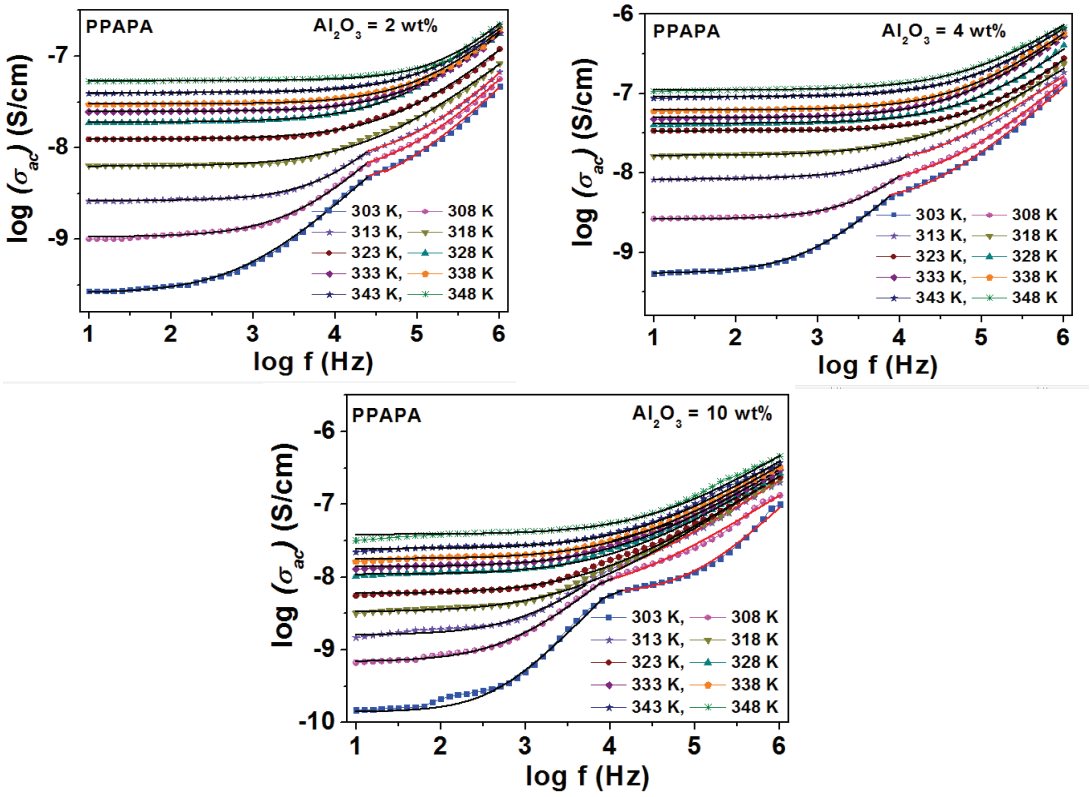

Fig. 5.4 (a) ac conductivity plots of blend specimens of PPAPA series at different temperatures

Interestingly, this phenomenon is commonly demonstrated by each nano-composite blend specimen of PPAPA series and is seen clearly visible through Fig. 5.4 (b) which shows variation in ac conductivity data with respect to logarithmic frequency values at different

concentrations of Al_2O_3. Dispersion frequency is observed to shift systematically towards higher frequency side with increasing temperature as seen from Fig. 5.4 (a). However, as evident from Fig. 5.4 (b), this dispersion frequency initially shifts towards higher frequency side with addition of Al_2O_3 nano-filler upto 6 wt% in the blends and then towards lower frequency side with its further addition.

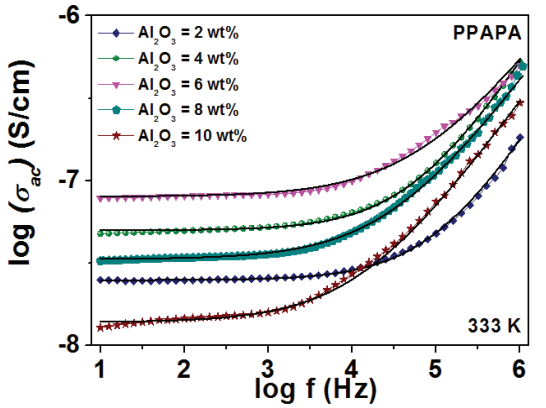

Fig. 5.4 (b) ac conductivity spectrum of blends of PPAPA series at different Al_2O_3 concentrations at 333 K

5.1.3 *ac Conductivity Scaling*

Further, temperature-wise scaling of these ac conductivity spectra of blend specimens of PPAP as well as PPAPA series is carried out and shown in Figs. 5.5 and 5.6, respectively. Scaling studies basically provide the better insight to the common underlying reason for a physical property. Moreover, scaling is one of the important features to evaluate any data. By changing the conductivity and frequency scale, we can obtain superimposed master curves for different conductivity isotherms to collapse into a common curve at all the considered temperatures. This further suggests that the process can be separated into a common physical mechanism which can be modified by thermodynamic scale only. This type of process is known as *'Time-Temperature Superimposition Principle (TTSP)'* [13]. Till date, different approaches have been adopted for scaling of the ac conductivity spectra especially, by **Summerfield** [14]**, Roling et al.** [15]**, Sidebottom** [14,15], **Ghosh** [16] and **Dyre** [17].

Summerfield approach is the simplest one that was used for scaling the ac conductivity spectra and is given as [18]:

$$\frac{\sigma'}{\sigma_0} = F\left(\frac{f}{\sigma_0 T}.x\right) \quad \ldots\ldots\ldots\ldots\ldots (5.1)$$

where, $f =$ frequency, $\sigma_0 =$ conductivity at any given temperature, $T =$ absolute temperature and $x =$ concentration factor.

Further, **Roling et al.** [15] have considered (i) $\sigma_{dc}\, T/x$ and (ii) $\sigma_{dc}\, T$ as compositions and scaling factors where, $T =$ absolute temperature, $\sigma_{dc} =$ dc conductivity and $x =$ mole fraction of mobile (alkali) ions [19]. On the other hand, **Sidebottom** [14,15,20] has considered the case where the content of alkali is quite low. In this case, the worker has made the use of the fact that ion hopping length changes with respect to the content of alkali. However, in this case, the shape of ac conductivity spectra is preserved even with changing temperature and the concentration of ions remains invariant. Here, the frequency is scaled by using the term '$\sigma_{dc}/\varepsilon_0\Delta\varepsilon$' where, $\sigma_{dc} =$ dc conductivity, $\varepsilon_0 =$ permittivity of free space and $\Delta\varepsilon = (\varepsilon_s - \varepsilon_\infty)$ is the change in permittivity from unrelaxed baseline 'ε_∞' to completely relaxed level 'ε_s' [19]. On the other hand, according to **Ghosh's** scaling model [16], the scaling approach is given by the relation as follows [19]:

$$\frac{\sigma'}{\sigma_{dc}} = F\left(\frac{\omega}{\omega_h}\right) \quad \ldots\ldots\ldots\ldots\ldots (5.2)$$

where, 'ω_h' is the hopping frequency and used as a scaling parameter for the frequency axis and $F =$ temperature independent universal function which describes dynamics of charge carriers.

In the present cases, the ac conductivity spectra are scaled using Almond-West conductivity formalism [13] given as:

$$\frac{\sigma'(\omega)}{\sigma_{dc}} = F\left(\frac{\omega}{\omega_h}\right) = \left[1 + \left(\frac{\omega}{\omega_h}\right)^n\right] \quad \ldots\ldots\ldots\ldots\ldots (5.3)$$

where, $\sigma'(\omega)$ = frequency dependent real part of conductivity, σ_{dc} = dc conductivity, $\omega = 2\pi f$ = angular frequency ('f' is expressed in Hertz), ω_h = hopping frequency and n = power law exponent or frequency exponent. This ac conductivity scaling done by using Almond-West formalism has also been carried out by **Khiar et al.** [13] in their chitosan-based polymer electrolyte system.

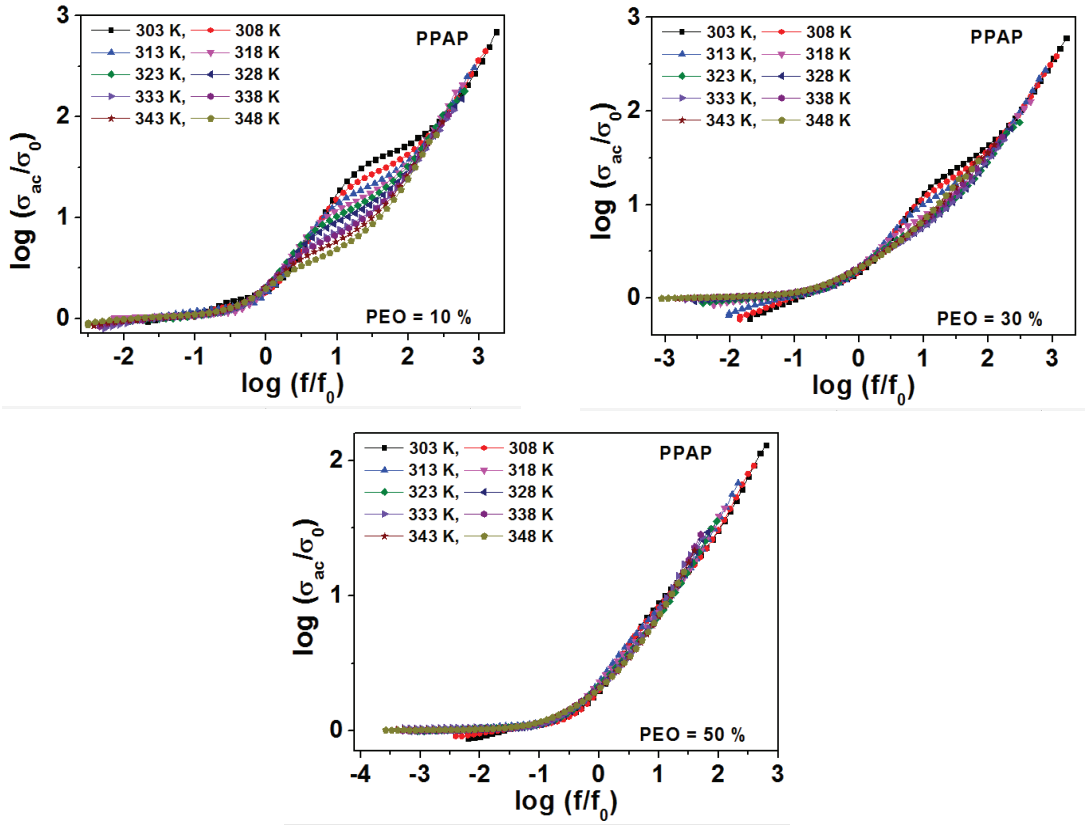

Fig. 5.5 Scaling of ac conductivity spectra of blend specimens of PPAP series at different temperatures

The temperature-wise scaled ac conductivity spectra of blends of PPAP and PPAPA series are depicted in Figs. 5.5 and 5.6, respectively. As observed from Fig. 5.5, for the blend specimen with 10 % of PEO, ac conductivity curves get almost perfectly overlapped but only at low frequency regions till dispersion frequency and at high frequency regions. At mid frequencies (beyond dispersion frequency region) these ac conductivity curves remain well separated from each other hence, depicting a prominent bumpy feature. With increasing content of PEO in blends ac conductivity curves in mid frequency region gradually come

closer to each other. However, the feature still continues to be clearly visible in the scaled ac conductivity spectra of the blend with 30% of PEO of PPAP series. But interestingly, at highest content of PEO of 50 %, ac conductivity spectra are observed to merge almost perfectly in the entire frequency range, yielding a single master curve. This discussion suggests that at lowest concentration of PEO, ion dynamics is unable to follow same mechanism throughout the temperature range as Ag^+ experience different environments to relax. But with further addition of PEO in blends, these Ag^+ gradually start experiencing the similar environments to relax. Finally, for the blend with 50 % of PEO, Ag^+ experience same environments to relax which further indicates that ion dynamics significantly follows same mechanism in the entire temperature range. Hence, *'Time-Temperature Superimposition Principle'* is followed, but only by the blend specimen with 50 % of PEO of PPAP series.

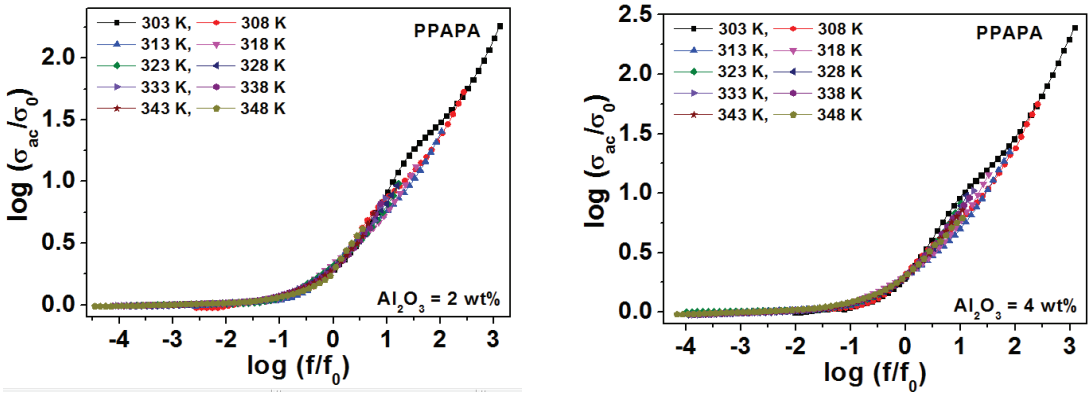

Fig. 5.6 Scaling of ac conductivity spectra of blend specimens of PPAPA series at different temperatures

On the contrary, as seen from Fig. 5.6, for nano-composite blends of PPAPA series, ac conductivity spectra are observed to get perfectly merged but only from low frequency region to dispersion frequency. At higher frequency, beyond the dispersion frequency, these ac conductivity curves are seen to remain well-separated. Hence, these nano-composite blends do not follow *'Time-Temperature Superimposition Principle'*.

Similarly, scaling of ac conductivity spectra of blends of respective PPAP and PPAPA series is carried out for different concentrations of PEO and Al_2O_3 respectively, using

Almond-West Formalism and depicted in Figs. 5.7 (a) and 5.7 (b), respectively. As observed from the Fig. 5.7 (a), ac conductivity data of blends of PPAP series are observed to remain separated in the high frequency range.

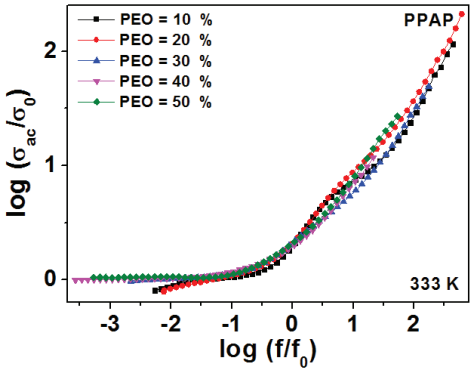

Fig. 5.7 (a) Scaling of ac conductivity spectrum of blends of PPAP series at different PEO concentrations at 333 K

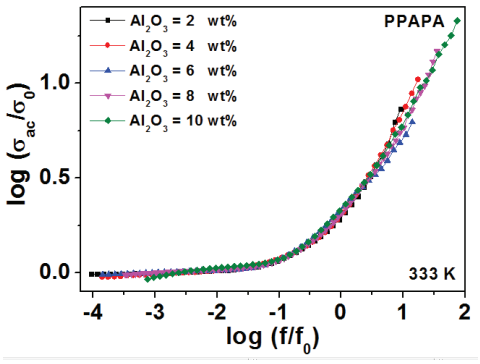

Fig. 5.7 (b) Scaling of ac conductivity spectrum of blends of PPAPA series at different Al_2O_3 concentrations at 333 K

On the other hand, in case of PPAPA series, ac conductivity data at all Al_2O_3 nano-filler concentrations show almost perfect overlapping in the entire frequency range as seen from the Fig. 5.7 (b). Hence, in case of the blends of PPAP series, ac conductivity spectra do not perfectly overlap to form a single master curve which indicates that ac conductivity scaling remains dependent of respective PEO concentrations whereas; ion dynamics follow same mechanism throughout the concentration range when Al_2O_3 is varied in the blend specimens of PPAPA series. Hence, PPAPA specimens follow *'Time-Concentration Superimposition Principle'*.

5.1.4 ***dc Conductivity Studies***

Further, ac conductivity spectra of blend specimens of PPAP and PPAPA series, as discussed previously, are fitted at all temperatures using *Jonscher's Power Law (JPL)* given as follows [21,22]:

$$\sigma'(\omega) = \sigma_{dc} + A\omega^{n} \quad \ldots\ldots\ldots\ldots\ldots (5.4)$$

Here, $\sigma'(\omega)$ = frequency dependent real part of conductivity, $\sigma_{dc} = \sigma_0$ = dc conductivity, A = pre-exponential constant, $\omega = 2\pi f$ = angular frequency ('f' is expressed in Hertz) and n = power law exponent or frequency exponent.

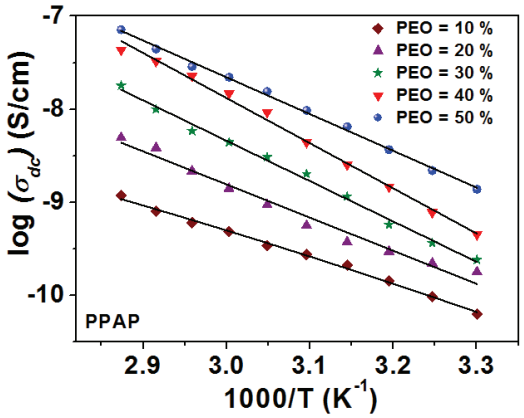

Fig. 5.8 (a) log σ_{dc} vs. 1000/T plot of blends of PPAP Series

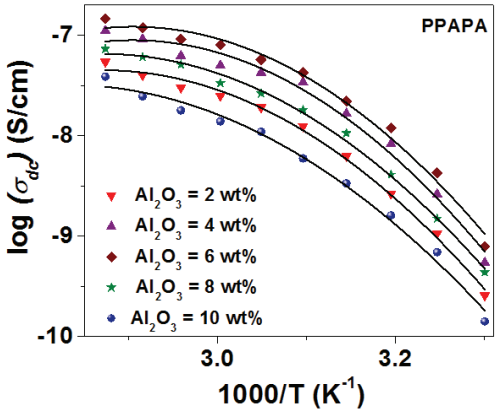

Fig. 5.8 (b) log σ_{dc} vs. 1000/T plot of of blends of PPAPA Series

Single relaxation feature appearing in every respective ac conductivity spectrum is fitted using single JPL equation whereas; the double relaxation feature is fitted separately by using two different JPL equations. Such a process of fitting of ac conductivity data is similarly carried out by **Mahato et al.** [23] for their double perovskite holmium zinc titanate (HZT) system. The fitting of ac conductivity data of blend specimens of PPAP and PPAPA series yields the values of dc conductivity in the entire temperature range of 303 K to 348 K. Such a variation in logarithmic values of dc conductivity (log σ_{dc}) is plotted against inverse of temperature for the blends of both PPAP and PPAPA series and depicted respectively, in the Figs. 5.8 (a) and 5.8 (b). At all the PEO concentrations, log 'σ_{dc}' values are observed to enhance linearly with temperature depicting linear or Arrhenius behaviour of dc conductivity with respect to temperature [24,25]. Such Arrhenius behaviour of dc conductivity with temperature is as also discussed by **Kesharwani et al.** [26] and **Karan et al.** [27]. On the contrary, for all the Al_2O_3 nano-filler based blend specimens, dc conductivity follows non-linear or Vogel-Tamman-Fulcher (VTF) type of behaviour with the temperature rise [25,26].

Such VTF behaviour of dc conductivity with temperature of the nano-filler 'based' blends of PPAPA series is quite different from the Arrhenius behaviour as depicted by the nano-filler 'free' blends of PPAP series. Hence, addition of various concentrations of Al_2O_3 nano-filler in the blend specimen with 50 % of PEO of PPAP series, changes the behaviour of dc conductivity from Arrhenius type to VTF type with the varying temperature. Such VTF type of conductivity behaviour with temperature is also observed in various composite polymer electrolyte systems studied by **Piszcz et al.** [28] and **Pradeepa et al.** [29].

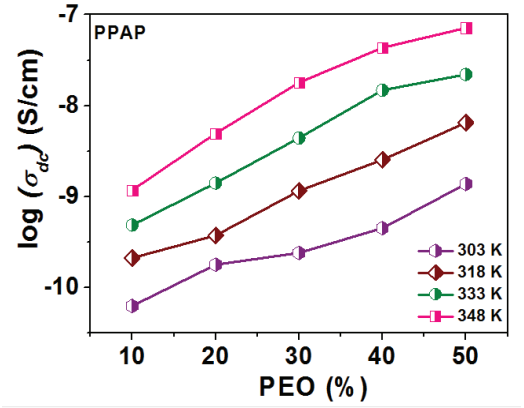

Fig. 5.9 (a) log σ_{dc} vs. PEO concentrations

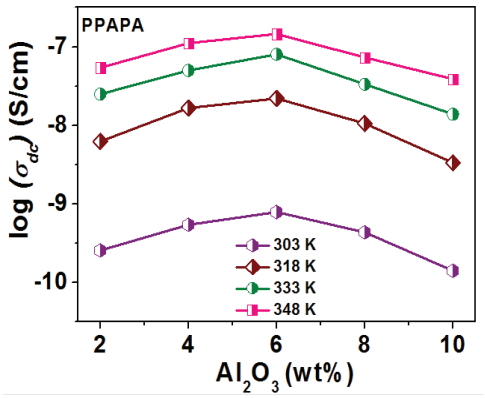

Fig. 5.9 (b) log σ_{dc} vs. Al_2O_3 concentrations

Commonly, in case of blends of both PPAP and PPAPA series, dc conductivity 'σ_{dc}' is observed to enhance considerably with the rising temperature. Basically, as temperature increases, polymer matrix expands easily which in turn gradually reduces its degree of crystallinity hence, enhancing amorphous phase and free volume therein. This creates pathways for dynamic and effortless mobility of ions, polymer segments and solvated molecules (in some cases) through the polymer matrix. As the amorphicity and hence, free volume and conducting pathways enhance with increasing temperature, the ionic and segmental mobility through the blend matrix also improves substantially which in turn leads to an increase in dc conductivity (σ_{dc}) with the temperature rise [30-33].

Further, logarithmic values of dc conductivity 'log σ_{dc}' is plotted with respect to PEO and Al_2O_3 concentrations at four different temperatures of the considered temperature range and depicted in Figs. 5.9 (a) and 5.9 (b), respectively. As seen from the Fig. 5.9 (a), the blend specimen with the least amount of PEO of 10 % depicts lowest conductivity. But with further addition of PEO polymer in blends, conductivity substantially enhances and becomes maximum at PEO = 50 %. Basically, content of viscous and rigid PVA is highest in the blend with lowest PEO content. Such viscous and rigid nature of PVA makes the matrix of PVA-PEO blend also highly viscous and rigid thus, increasing its crystallinity. This not only hinders polymeric segmental motions but also the mobility of Ag^+ and NO_3^- charge carriers therein. Owing to this reason, the blend with least PEO content and optimum PVA concentration shows lowest conductivity. But with the addition of PEO in these blends, conductivity of blends substantially enhances. Basically, PEO chains are flexible and hence, when mixed with stiff chained structured PVA polymer, improves the flexibility of the blend matrix thus, promoting ion transport and segmental motion therein. Hence, higher the amount of flexible chained PEO polymer and lower the concentration of viscous, rigid and stiff chained PVA polymer in the blend matrix, higher is the ionic and segmental mobility and hence, higher is the dc conductivity 'σ_{dc}'.

On the other hand, with the addition of Al_2O_3 nano-filler in blend specimens of PPAPA series, dc conductivity 'σ_{dc}' values enhance considerably but only upto Al_2O_3 = 6 wt% as also seen from Fig. 5.9 (b). With further addition of Al_2O_3, dc conductivity values of the blends drop down substantially. In this case, at lower Al_2O_3 concentrations, nano-filler particles are well-separated from each other. Hence, these filler particles are easily able to perturb the packing of polymer chains and make the blend matrix highly amorphous. With the progress of this process polymeric chains become more dynamic and flexible thus, enhancing matrix's flexibility. Further, according to the suggestion of **Choudalakis et al.**

[34], incorporation of filler particles in a suitable proportion into the polymeric matrix also influences free volume therein rather, often enhances it thus, forming conducting pathways for easy mobility of free charge carriers and polymeric chain segments. In the present case also, all these phenomena are expected to occur prominently with the initial addition of Al_2O_3 in blends which in turn promote easy mobility of polymer chain segments along with Ag^+ and NO_3^- in the blend matrices [30]. But Al_2O_3 nano-filler when dispersed beyond 6 wt% in the blend matrix, form the neutral aggregates which in turn block the conducting pathways, hamper the mobility of charge carriers and reduce conductivity of the polymeric system [5,29,30,34-44]. This suggests that out of all the nano-composite blends of PPAPA series, the one with 6 wt% of Al_2O_3 nano-filler depicts optimum dc conductivity (σ_{dc}).

5.1.5 ***Conduction Hopping Frequency***

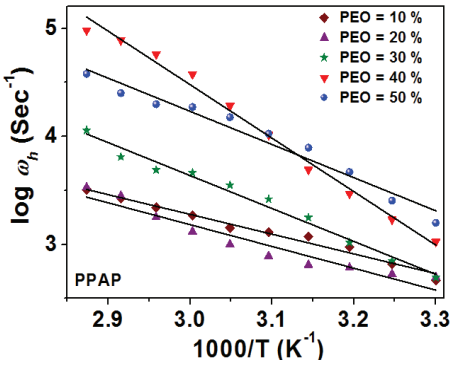

Fig. 5.10 (a) log ω_h vs. 1000/T plot of blends of PPAP series

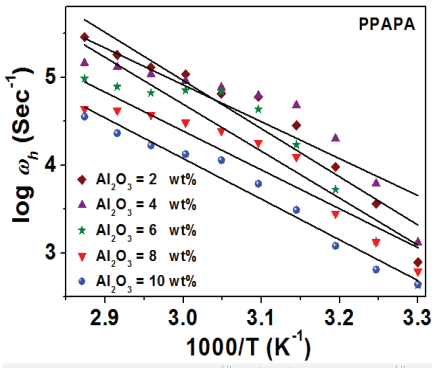

Fig. 5.10 (b) log ω_h vs. 1000/T plot of blends of PPAPA series

Fitting of ac conductivity data of respective blend specimen of PPAP and PPAPA series done using Jonscher's Power Law (JPL) equation also provides the values of power law exponent 'n' and constant 'A' for each respective blend specimen at the respective temperatures. By substituting the respective values of 'n' and 'A' along with dc conductivity 'σ_{dc}' in the following equation, the respective values of *'Conduction Hopping Frequency*

(ω_h)' can be obtained for each respective Ag^+ conducting blend specimen at all the temperatures [22,45,46].

$$\omega_h = \left(\frac{\sigma_{dc}}{A}\right)^{\frac{1}{n}} \quad \ldots\ldots\ldots\ldots\ldots (5.5)$$

Variation in the logarithmic values of conduction hopping frequency (log ω_h) with inverse of temperature for each respective blend specimen of PPAP and PPAPA series is shown in Figs. 5.10 (a) and 5.10 (b), respectively. As seen from both these figures, for each of the Ag^+ conducting blend specimens, 'log ω_h' values enhance linearly with the rising temperature. Such Arrhenius relation of 'log ω_h' with respect to temperature suggests that conduction hopping frequency is a thermally activated process.

5.1.6 ***Modulus Studies***

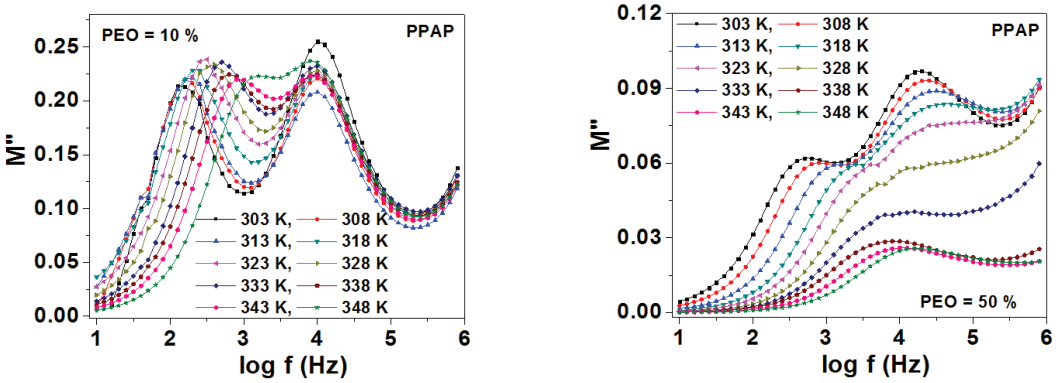

Fig. 5.11 (a) Modulus spectra of blend specimens of PPAP series at different temperatures

Investigation of electric modulus (M") of blends of PPAP and PPAPA series is carried out in order to understand their relaxation dynamics. Temperature-wise plots showing variation in imaginary parts of modulus (M") with respect to logarithmic values of frequency (log f) for the blends of PPAP and PPAPA series are depicted in Figs. 5.11 (a) and 5.12 (a), respectively. As observed from the modulus spectra of respective blend specimens of PPAP as well as PPAPA series, M" values remain low and constant at low frequency region. Basically, at low frequencies, charge carriers are mobile over long distances. Such charge

carrier mobility is facilitated under the action of an induced electric field thus, supporting long range motion of charge carriers (ions). But as the frequency increases, these charge carriers get confined to the potential wells and hence, get mobile only over shorter distances. Hence, there occurs transition from long range to short range mobility of charge carriers which in turn leads to the formation of peak feature in the modulus spectrum with the increasing frequencies. All these phenomena are said to be due to material's bulk effect [47,48]. The modulus spectra of the respective blend with 10 % of PEO show presence of double relaxation feature at each temperature wherein; two relaxation peaks appear at two different frequencies. The first relaxation peak appears at low-mid frequency region whereas; the second one lies in mid-high frequency range. Similar feature as observed in the present cases is also noticed by **Castillo et al.** [49] in their as studied electrolyte system. Such a double relaxation feature appearing in modulus spectra of the present case is similar to that appearing in the previously discussed ac conductivity studies. Hence, the feature can be said to correspond to the heterogeneity in polymer matrix which lead to immiscibility of both the host polymers with each other. However, at 50 % of PEO, two relaxations still occur prominently but only at lower temperatures. At higher temperatures, only the relaxation at low-mid frequency region persists whereas; the one at mid-high frequencies gradually suppresses with increasing temperatures.

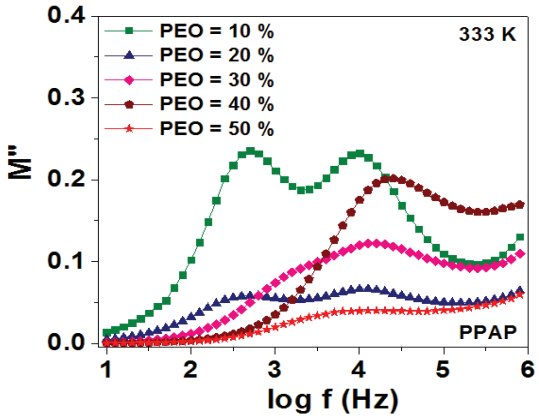

Fig. 5.11 (b) Modulus spectrum of blends of PPAP series at different PEO concentrations at 333 K

Also, as observed from Fig. 5.11 (b), modulus curve for the blend specimen with 10 % of PEO shows the presence of two different relaxation peaks at respective low-mid and mid-high frequencies. However, at 20 % of PEO, one of the relaxations of this double relaxation feature starts disappearing thus, yielding a single relaxation feature for blends with higher contents of PEO of 30%, 40 % and 50 %. This indicates that at lower levels of PEO, the PVA and PEO host polymers are not considerably compatible and miscible with each other. This leads to the individual relaxation peaks corresponding to the independent PVA and PEO rich phases in the modulus spectra. With the gradual addition of PEO in blends, miscibility and compatibility amongst the host polymers improve substantially. This results in the formation of a single homogeneous PVA-PEO blend phase which leads to a single relaxation feature in the modulus spectrum.

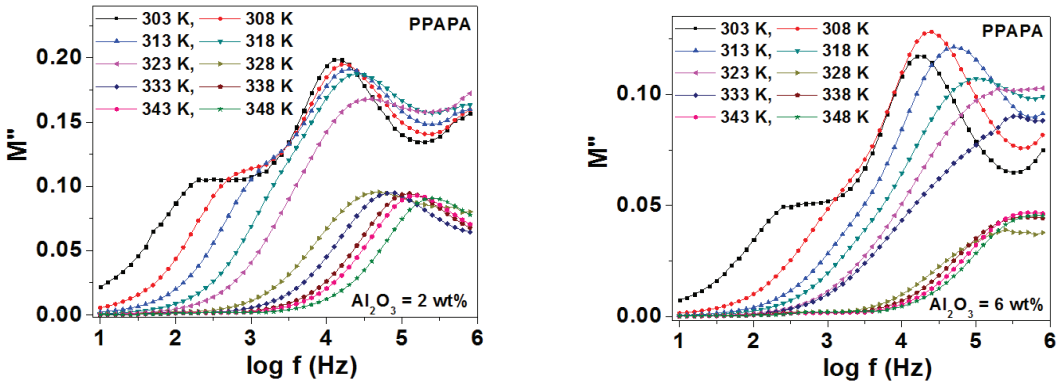

Fig. 5.12 (a) Modulus spectra of blend specimens of PPAPA series at different temperatures

Similar double relaxation feature is observed to occur at lower temperatures in M" vs. log f spectra of blend specimens of PPAPA series as seen from Fig. 5.12 (a). But at higher temperatures, only low-mid frequency relaxation is prominently present whereas; the one at mid-high frequencies gets completely suppressed. Interestingly, in the temperature-wise modulus spectra corresponding to the blend specimens of both PPAP as well as PPAPA series, frequency corresponding to the peak maxima is observed to shift consistently towards higher frequency side with rising temperature which indicates that ionic relaxation is a

thermally activated process [47]. However, incorporation of Al_2O_3 nano-filler in blends from 2 wt% to 10 wt% leads to the formation of a single and homogeneous PVA-PEO blend phase even at lower temperatures. This is clearly visible from the modulus spectrum as shown in Fig. 5.12 (b).

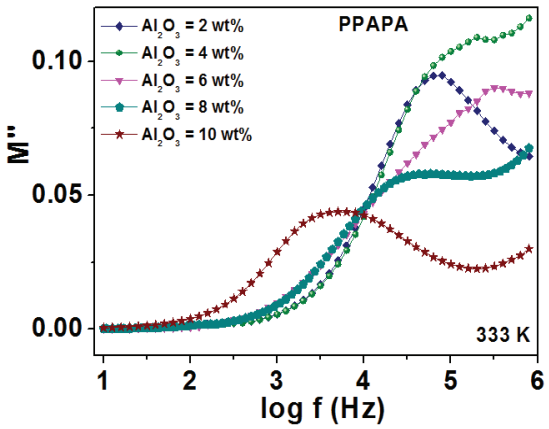

Fig. 5.12 (b) Modulus spectrum of blends of PPAPA series at different Al_2O_3 concentrations at 333 K

Moreover, with the initial addition of Al_2O_3 upto 6 wt% in blends, the peak maxima shift gradually towards higher frequency side. However, at Al_2O_3 > 6 wt%, the reverse phenomenon takes place.

5.1.7 ***Modulus Scaling***

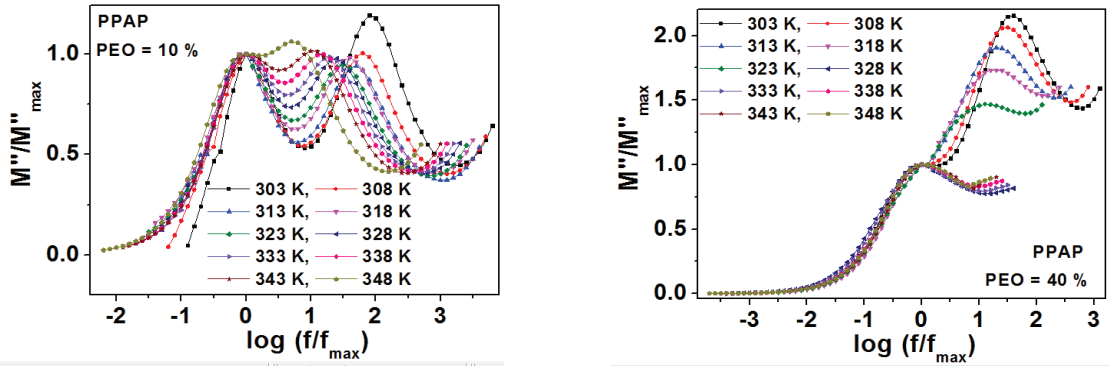

Fig. 5.13 (a) Scaling of modulus spectra of blend specimens of PPAP series at different temperatures

Further, temperature-wise scaling of these modulus spectra of blends of both PPAP as well as PPAPA series is done and depicted in respective Figs. 5.13 (a) and 5.13 (b). As

observed from each of the figures, data of modulus spectra of none of the blend specimens of either of PPAP or PPAPA series get perfectly overlapped. In each case, presence of double relaxation feature in modulus spectra limits the perfect merging of modulus curves to form a single master curve. This suggests that in case of blend specimens of both PPAP as well as PPAPA series relaxation dynamics does not follow *'Time-Temperature Superimposition Principle'* [30].

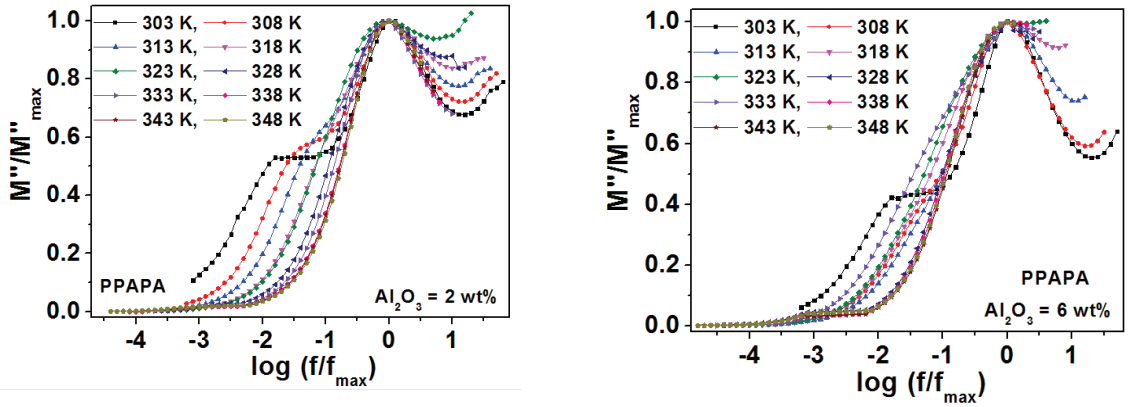

Fig. 5.13 (b) Scaling modulus spectra of blend specimens of PPAPA series at different temperatures

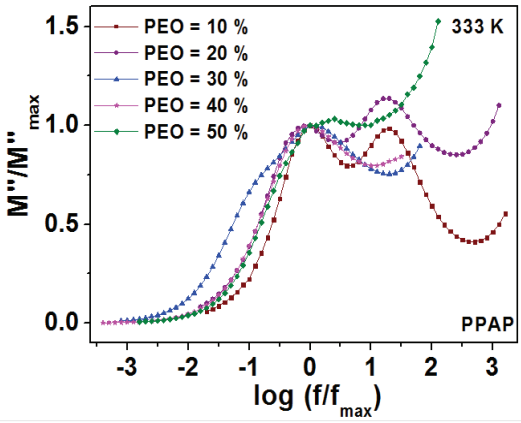

Fig. 5.14 (a) Scaling of modulus spectrum of blends of PPAP series at different PEO concentrations at 333 K

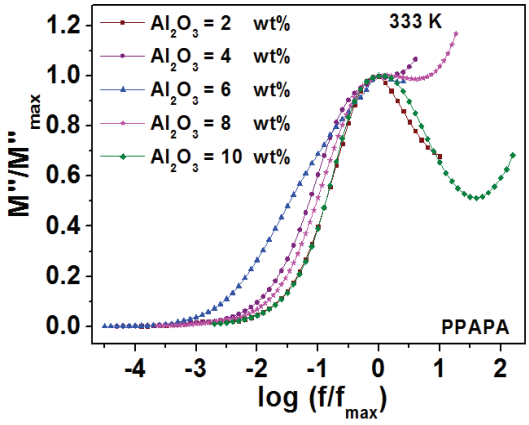

Fig. 5.14 (b) Scaling of modulus spectrum of blends of PPAPA series at different Al_2O_3 concentrations at 333 K

Further, scaling of modulus spectra is carried out at different PEO and Al_2O_3 compositions and shown in Figs. 5.14 (a) and 5.14 (b), respectively. Fig. 5.14 (a) shows that modulus curves of blends of PPAP series do not perfectly overlap on each other to yield a

single master curve. Similarly, modulus spectra of nano-composite blends of PPAPA series, as seen from Fig. 5.14 (b), also do not coalesce perfectly. This infers that in both, PPAP as well as PPAPA series, relaxation dynamics respectively depend on PEO and Al_2O_3 concentrations and hence, is unable to follow *'Time-Concentration Superimposition Principle'*. Similar observations are reported by **Gondaliya et al.** [42], in their PEO based polymeric system.

5.1.8 ***Relaxation Time***

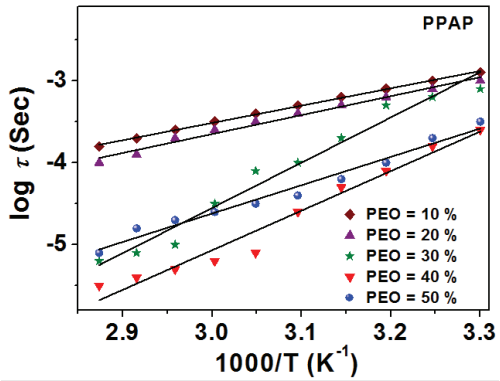

Fig. 5.15 (a) log τ vs. 1000/T plot of blends of PPAP series

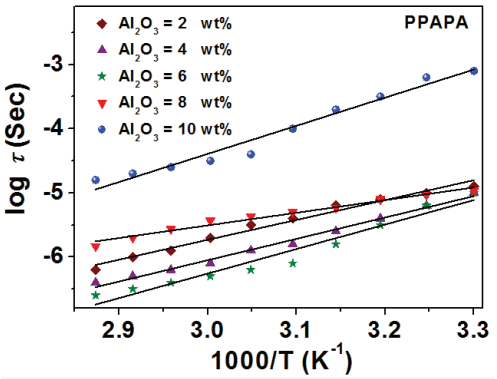

Fig. 5.15 (b) log τ vs. 1000/T plot of blends of PPAPA series

Values of maximum frequency 'f_{max}' corresponding to peak maxima of respective temperature-wise modulus spectra of blends of PPAP and PPAPA series are used to calculate respective relaxation time 'τ' values by using the following equation.

$$\tau = \frac{1}{2\pi f_{max}} \qquad \ldots\ldots\ldots\ldots\ldots (5.6)$$

Variation in the logarithmic relaxation time 'log τ' values of the respective blend specimens of PPAP and PPAPA series, is plotted with respect to inverse of temperature and shown in Figs. 5.15 (a) and 5.15 (b), respectively. As observed from both these figures, 'log τ' values decrease linearly with the rise in temperature. This suggests that relaxation time follows Arrhenius law. Moreover, the linear variation in 'log τ' values with respect to temperature further indicates that relaxation time is a thermally activated process [50-55].

5.1.9 *Dielectric Studies*

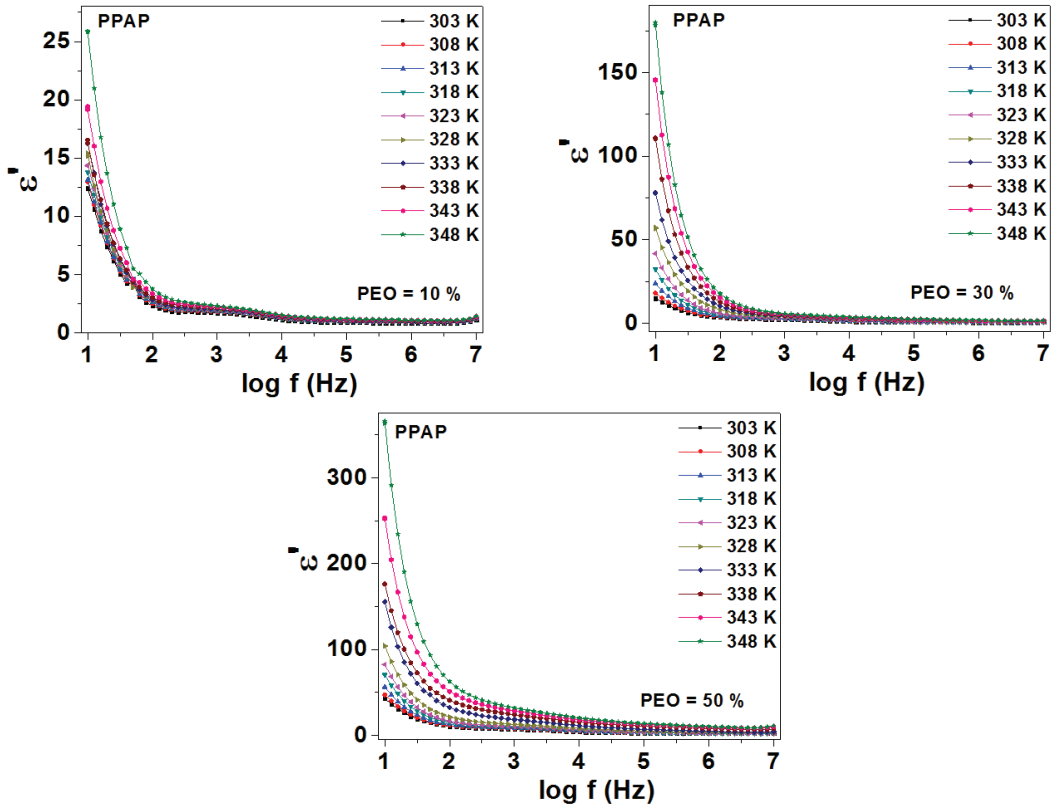

Fig. 5.16 (a) ε' vs. log f spectra of blend specimens of PPAP series at different temperatures

Dielectric properties of the blend specimens of PPAP and nano-composite PPAPA series can be well understood by investigating their dielectric parameters which mainly include dielectric constant (ε') and dielectric loss (ε"). Temperature-wise plots of dielectric constant (ε') vs. logarithmic values of frequency (log f) of the blends of PPAP and PPAPA series have been depicted in Figs. 5.16 (a) and 5.16 (b), respectively. As observed from the plots, values of dielectric constant (ε') are found to be highest at lowest frequency. But as the frequency increases, these ε' values drop systematically. Finally, beyond a certain frequency termed as *'Dispersion Frequency'*, ε' values get low and remain almost constant with further rise in frequency. Similar trend is also followed by dielectric loss (ε") with respect to logarithmic values of frequency (log f) as seen from temperature-wise ε" vs. log f plots depicted in Figs. 5.17 (a) and 5.17 (b) for respective blends of PPAP and PPAPA series.

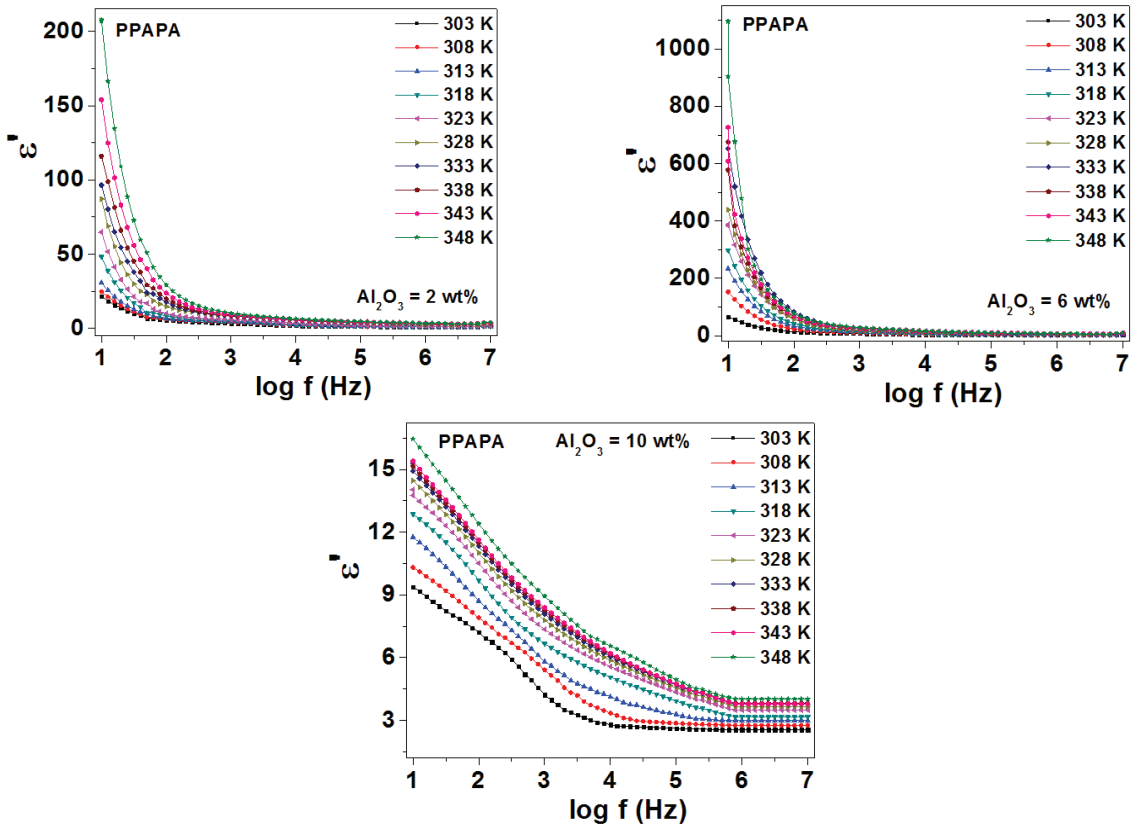

Fig. 5.16 (b) ε' vs. log f spectra of blend specimens of PPAPA series at different temperatures

Basically, at lower frequencies, dipoles of the macromolecules get enough time to orient themselves in the direction of applied electric field. Also, the charge carriers (ions) can immediately get accumulated at the electrode-electrolyte interfacial regions leading to space charge effects which are mainly due to different types of polarization including electronic, dipolar, ionic and spatial charge contribution [11,30,56,57]. As all these phenomena get considerably prominent as the frequency reduces. Hence, the values of dielectric constant (ε') and dielectric loss (ε") enhance with decreasing frequency. Such a variation in dielectric constant (ε') with frequency can be attributed to the formation of space charge region at the electrode and electrolyte interface which is also known as $(\omega)^{n-1}$ variation of non-Debye behaviour. Hence, the presence of such a polarization effect also indicates non-Debye type of behaviour [8].

But as frequency increases beyond dispersion frequency, these dipoles of macromolecules experience difficulty to cope up with the direction of applied electric field owing to its quick reversal. Moreover, migration of ions also mitigates with rising frequency. In other words, as frequency increases beyond dispersion frequency, the applied electric field reverses so rapidly that it not only becomes highly difficult for the dipoles of the macromolecules to orient themselves in the direction of applied electric field but also the diffusion of ions in the applied field's direction lessens down. All these factors in turn lead to decrease in polarization and hence, drop in the values of dielectric constant (ε') as well as dielectric loss (ε") at frequencies higher than dispersion frequency [30,58,59]. Hence, at frequencies > dispersion frequency, these ε' and ε" values remain low and constant with respect to frequency.

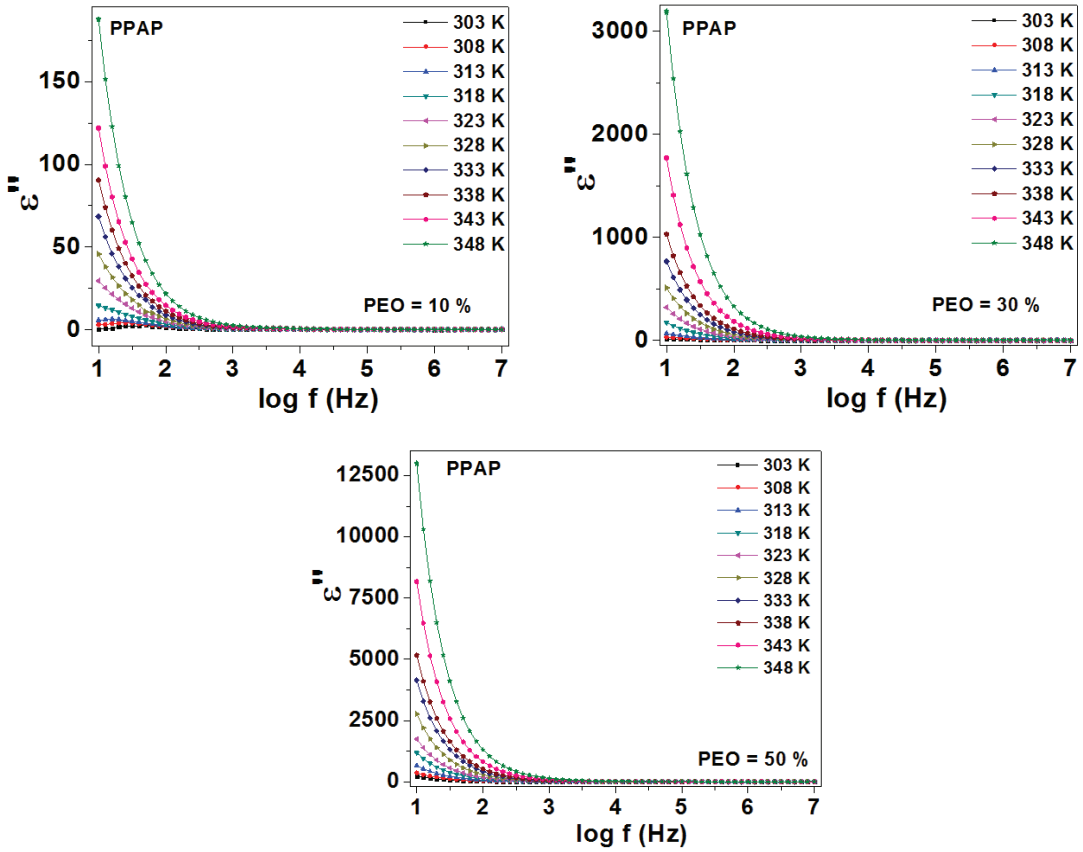

Fig. 5.17 (a) ε" vs. log f spectra of blend specimens of PPAP series at different temperatures

In addition to this, Figs. 5.16 (a) and (b) and Figs. 5.17 (a) and (b) indicate that at any particular frequency below dispersion frequency, values of both dielectric constant (ε') as well as dielectric loss (ε") enhance systematically with rising temperature because of the thermal activation of the charge and energy requirement for the transition of ions from one site to another. Here, dielectric loss (ε") is the direct measure of energy dissipated and it generally contributes in the ionic transport and the polarization of the charges or the dipoles. As the processes of orientation of dipoles and transport of free charge carriers get substantially active with increasing temperature, the amount of energy lost in their occurrence also increases automatically. This is clearly visible in the form of rise in the values of dielectric loss (ε") with increasing temperature (at a specific frequency < dispersion frequency). Hence, ion jumps and dc conduction losses of ions along with polarization losses contribute in increasing values of dielectric loss (ε") with rising temperature.

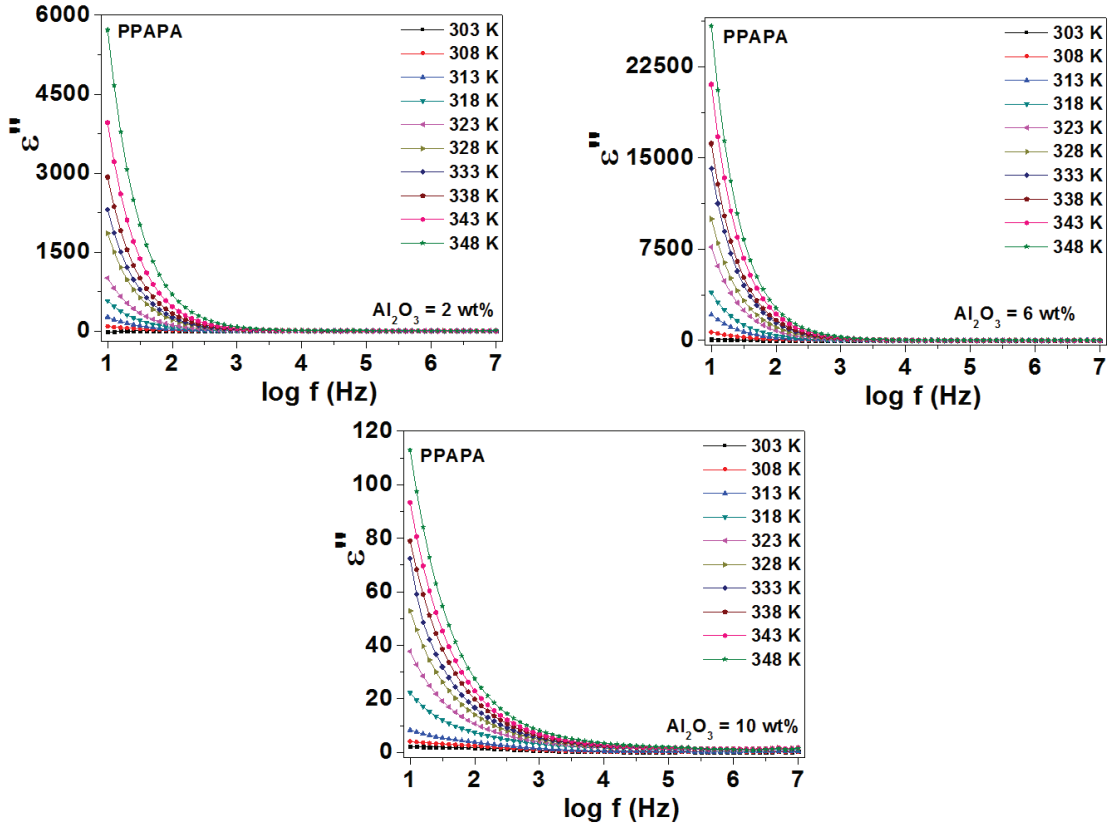

Fig. 5.17 (b) ε" vs. log f spectra of blend specimens of PPAPA series at different temperatures

But all these processes can successfully take place only at frequencies lower than dispersion frequency due to slow reversal of electric field. Beyond dispersion frequency, reversal of electric field occurs too rapid to build up free charge carriers at electrode-electrolyte interfaces and to orient the dipoles of macromolecules in the electric field's direction. However, no dielectric loss peaks are observed in any of the ε" vs. log f spectra owing to dominating dc conductivity [57,60].

In addition to these features, dispersion frequency in the respective ε' vs. log f spectra as well as ε" vs. log f spectra of blend specimens of each series shifts gradually towards higher frequency side with increasing temperature. Here, as temperature increases, relaxation of polymer chain segments gets substantially faster. This further introduces flexibility in polymer chain segments and hence, their mobility. Moreover, mobility of free charge carriers (ions) increases under the action of externally applied electric field hence, leading to such a shift in dispersion frequency towards higher frequency side with the rising temperature.

Interestingly, at each particular frequency below dispersion frequency, values of both dielectric constant (ε') and dielectric loss (ε") enhance considerably with the addition of PEO in blends. Basically, PEO polymer possesses ether linkages with oxygen atoms in its structure. Due to local motion of the side group dipoles about the main backbone of the polymer, loss increases. Moreover, transient crosslinks possibly occur between Ag^+ and ether oxygen of PEO. As the amount of PEO increases, more and more such transient crosslinks are formed between Ag^+ and PEO's ether oxygen. This makes dissociation process of $AgNO_3$ salt highly active thus, enhancing number of free Ag^+ for conduction process [24,26,61-69]. Hence, the number of these free Ag^+ and NO_3^- building up at the electrode-electrolyte interfaces also increases thus, enhancing ε' and ε" values with PEO concentration. Also, at each particular frequency < dispersion frequency, values of both ε' and ε" vary in the similar fashion with respect to Al_2O_3 concentration as depicted by dc conductivity.

5.2 Li^+ Conducting Blend Polymer Electrolyte Systems

5.2.1 *Impedance Studies*

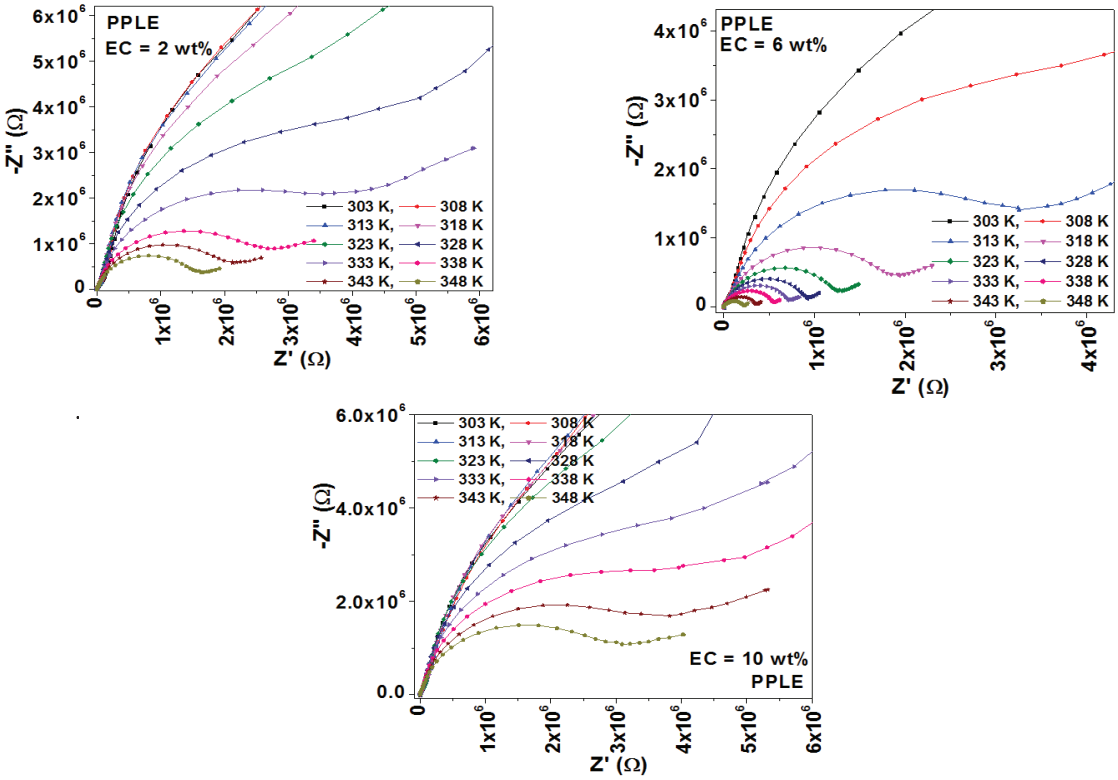

Fig. 5.18 (a) Nyquist plots of blend specimens of PPLE series at different temperatures

First Li^+ conducting series is PPLE series given as '[$PVA_{(50)}$: $PEO_{(50)}$] – 5 wt% $LiCF_3SO_3$ – x wt% EC'. In order to understand the effect of EC plasticizer, Nyquist plots of the blend specimens of this series as shown in Fig. 5.18 (a) plotted at different temperatures are investigated in detail.

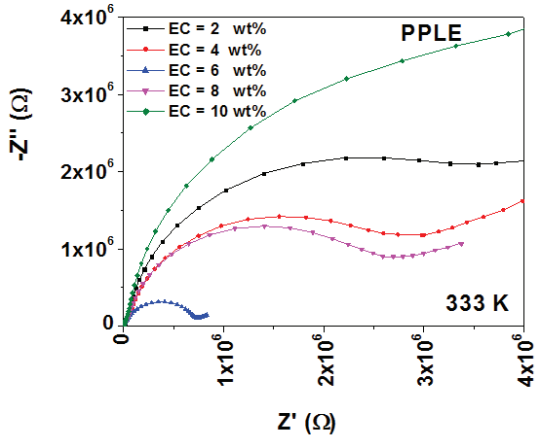

Fig. 5.18 (b) Nyquist plot of blends of PPLE series at various EC concentrations at 333 K

As seen from the figures, at various concentration of EC plasticizer, Nyquist plots show the presence of a semicircle at high frequency region followed by a spike/spur at lower frequency side and this is a common characteristic feature usually depicted by an ion conducting polymer electrolyte [56]. Also, intercept of real axis shifts systematically towards origin with increasing temperature which suggests the substantial drop in bulk resistance (R_b) of EC plasticized blend specimens with rising temperature.

Further, in EC concentration-wise Nyquist plot as depicted in Fig. 5.18 (b), intercept of real axis (Z') of the semicircles initially shifts towards origin with increasing amount of EC plasticizer in blends upto 6 wt%, indicating gradual drop in their bulk resistance 'R_b'. But with further incorporation of EC in blends, this intercept of real axis gradually shifts away from the origin, showing increase in the 'R_b'.

Next, lithium salt ($LiCF_3SO_3$) is varied from 3 wt% to 11 wt% in the blend with 6 wt% of EC of PPLE series as it depicts minimum bulk resistance as compared to rest of the blends of this series. Nyquist plots plotted in the temperature range of 303 K to 348 K of all the blends of this PPEL series given as '[$PVA_{(50)}$: $PEO_{(50)}$] – 6 wt% EC – x wt% $LiCF_3SO_3$' are as shown in Fig. 5.19 (a). But for blend specimens of this series, Nyquist plots show presence of only semicircle at higher frequency region whereas; the spike/spur is completely absent in these plots. Each Nyquist plot shows substantial shift of intercept of real axis towards origin with rising temperature. This suggests that as temperature increases, bulk resistance of blend specimens of PPEL series systematically drops down.

On the other hand, in Nyquist plot as shown in Fig. 5.19 (b), plotted at 333 K for blends at various $LiCF_3SO_3$ concentrations, intercept of real axis (Z') of semicircular arcs initially, shifts towards origin with increasing amount of salt in blends. But at 11 wt% of $LiCF_3SO_3$, this intercept of real axis shifts away from origin. It means that with increasing content of salt

upto 9 wt%, bulk resistance of the blend specimens gradually decreases. But beyond 9 wt% of salt, the reverse phenomenon occurs.

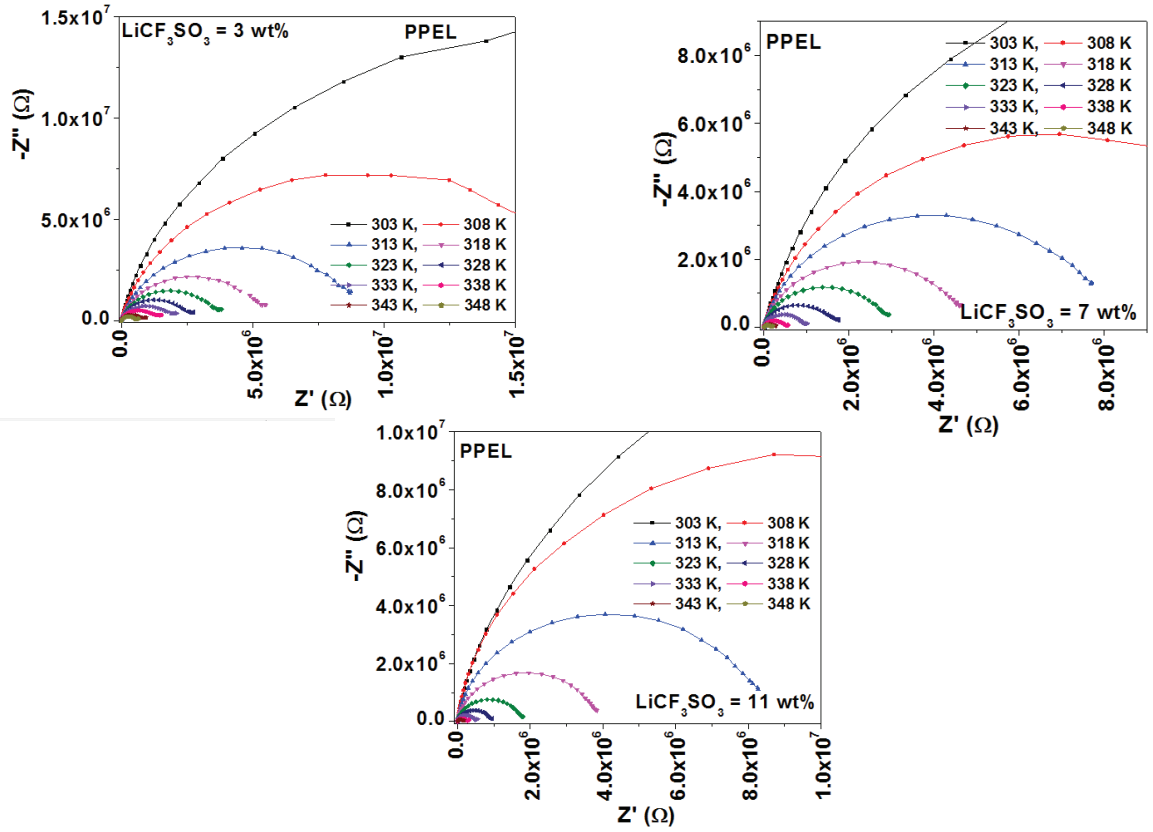

Fig. 5.19 (a) Nyquist plots of blend specimens of PPEL series at different temperatures

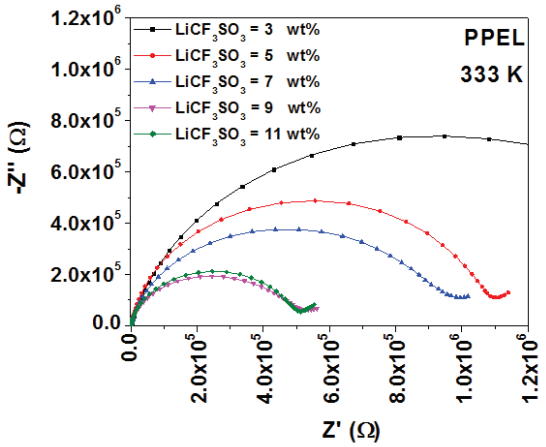

Fig. 5.19 (b) Nyquist plot of blends of PPEL series at various $LiCF_3SO_3$ concentrations at 333 K

In this blend with 9 wt% $LiCF_3SO_3$ salt depicting least 'R_b' as compared to other blends of PPEL series, we dispersed Al_2O_3 nano-filler whose concentration is varied from 2 wt% to

10 wt% to form the nano-composite blend series given as '[$PVA_{(50)}$: $PEO_{(50)}$] – 6 wt% EC – 9 wt% $LiCF_3SO_3$ – x wt% Al_2O_3'. Temperature dependent Nyquist plots depicting semicircles at higher frequency side for blends of this series are shown in Fig. 5.20 (a). As observed from these Nyquist plots, intercept of real axis (Z') shifts systematically towards origin as temperature increases. This indicates continuous reduction in bulk resistance of nano-composite blends with rising temperature.

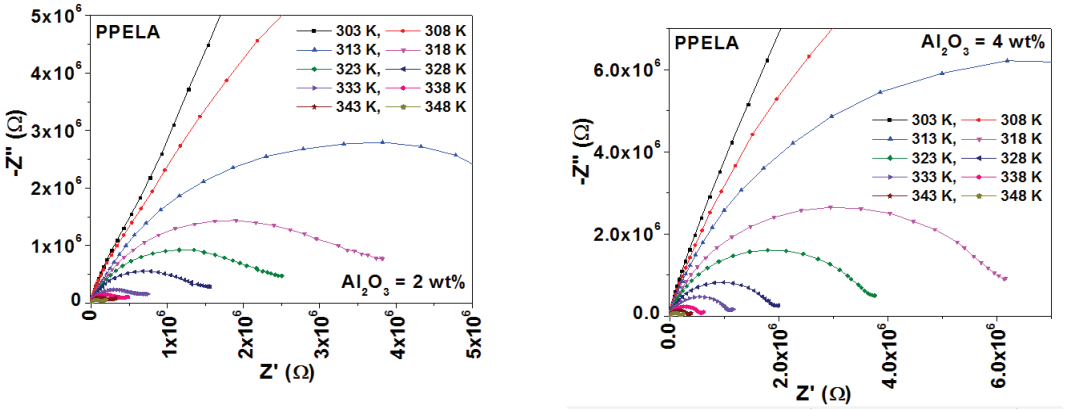

Fig. 5.20 (a) Nyquist plots of blend specimens of PPELA series at different temperatures

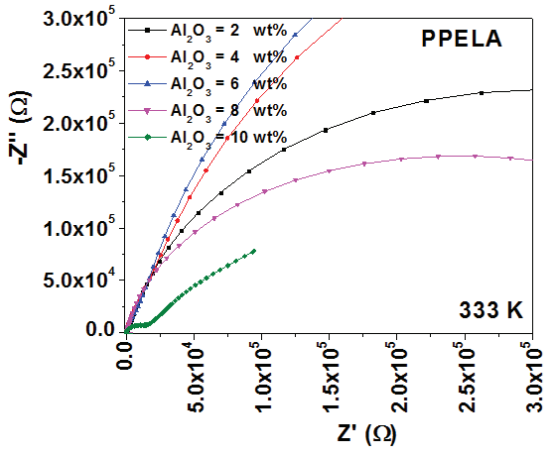

Fig. 5.20 (b) Nyquist plot of blends of PPELA series at various Al_2O_3 concentrations at 333 K

However, in Al_2O_3 concentration-wise plotted Nyquist plot as shown in Fig. 5.20 (b), the intercept of real axis (Z') of the semicircles shifts away from the origin with the initial addition of Al_2O_3 in blends upto 6 wt% hence, indicating the gradual increment in 'R_b'. However, at Al_2O_3 > 6 wt%, this intercept of real axis (Z') shifts towards origin. This suggests the systematic reduction in bulk resistance of nano-composite blends but beyond a

certain concentration of 6 wt% of Al_2O_3 therein. Such a phenomenon as shown by the nano-composite blends of Li^+ conducting PPELA series is completely reverse to that depicted by the nano-composite blends of Ag^+ conducting PPAPA series.

5.2.2 *ac Conductivity Studies*

Using these complex impedance data, temperature-wise ac conductivity spectra of blends in which EC plasticizer, $LiCF_3SO_3$ salt and Al_2O_3 nano-filler have been varied are plotted and shown in Figs. 5.21 (a), 5.22 (a) and 5.23 (a), respectively.

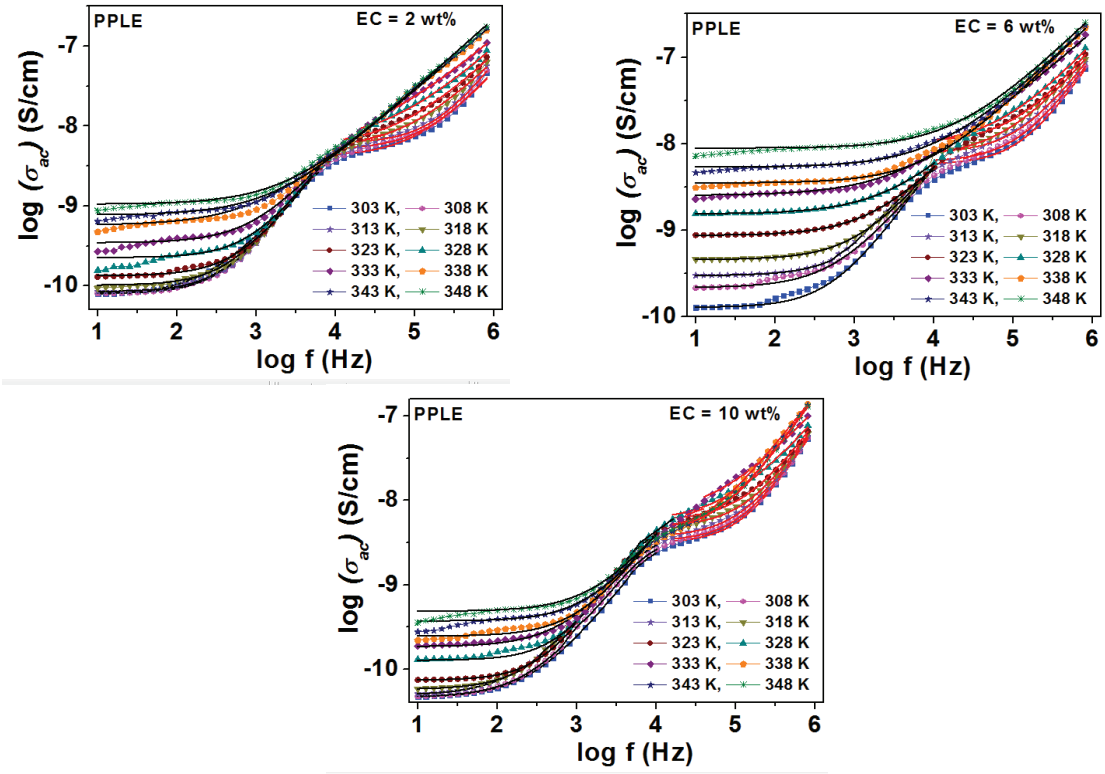

Fig. 5.21 (a) ac conductivity plots of blend specimens of PPLE series at different temperatures

As seen from each figure, conductivity remains low and constant at low frequency regions. This is frequency independent conductivity and is also termed as *'dc Conductivity'*. But beyond dispersion frequency, also known as hopping frequency, conductivity is observed to enhance significantly with increasing frequency, showing frequency dependent nature. This frequency dependent conductivity can be termed as *'ac Conductivity'* which usually

takes place due to release of trapped charge carriers at appreciably high frequencies. It is observed that ac conductivity increases with increase in frequency at all temperatures. Hence, such frequency dependent real part of ac conductivity show two distinct regions i.e. frequency independent plateau followed by a high frequency dispersion region. Here, the low frequency region is attributed to long range ionic mobility and high frequency region is ascribed to short range (hopping) ionic motion. Moreover, as observed from each ac conductivity plot, hopping frequency systematically shifts towards higher frequency side with increasing temperature. Such a phenomenon possibly occurs due to increased segmental motion of polymer chains and increased mobility of ions [58,70,71].

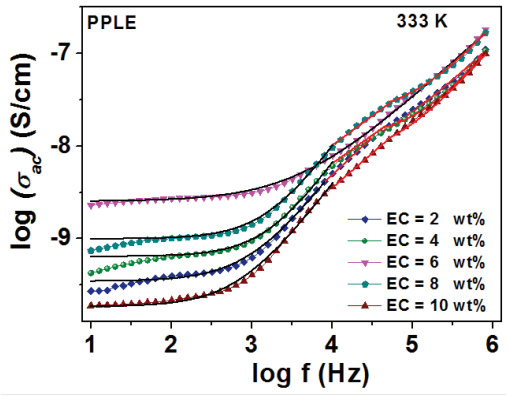

Fig. 5.21 (b) ac conductivity spectrum of blends of PPLE series at different EC concentrations at 333 K

However, as observed from ac conductivity plot of Fig. 5.21 (a), ac conductivity curves show presence of a double step-like feature corresponding to two different relaxations occurring at two different frequencies but only at low temperatures nearby PEO's melting temperature. Such a double relaxation feature as observed in ac conductivity spectra of present EC plasticized PVA-PEO blend specimens is also seen and studied by **Sharma et al.** [72] in their EC plasticized PEO-PMMA-$AgNO_3$ blend polymer electrolyte system. This suggests that in the present case, inspite of incorporation of EC plasticizer, the two host polymers i.e. PVA and PEO remain slightly incompatible with each other. Such behaviour is due to inherent inhomogeneous nature of the specimen below melting temperature of PEO,

which leads to the own individual relaxation features of corresponding PVA and PEO host polymers. At and beyond melting temperature of PEO (~ 60 °C or 333 K), the mid-frequency hump gradually vanishes whereas; only low frequency relaxation feature remains present. To quantitatively describe the ion conduction process, generally the emphasis is given on frequency independent plateau and high frequency dispersion regions. This behaviour follows the universal Jonscher's Power law given as:

$$\sigma' = \sigma_{dc} + Af^{n} \quad \ldots\ldots\ldots\ldots\ldots (5.7)$$

Here, $\sigma' \rightarrow \sigma_{dc}$, $A \rightarrow f$ and $0 \leq n \leq 1$. In general, for ionic conductors, this value lies from 0.4 to 0.7. These ac conductivity plots are fitted using Jonscher's Power Law (JPL) formula to obtain respective 'σ_{dc}' values at different temperatures and all these plots are found to be reasonably good fitted. As per jump relaxation model, an ion jumps from one site to its neighbouring favourable site contributing towards dc conductivity when frequencies are low. But as the frequency is increased, the correlated forward-backward hopping of mobile ions give rise to ac conductivity due to short time period. On the other hand, as temperature approaches to melting temperature of PEO, this PEO polymer melts and forms a single and homogenous PVA-PEO blend phase. Such a single PVA-PEO blend phase corresponds to single relaxation feature in ac conductivity spectra of blend specimens of PPLE series at higher temperatures as also seen from Fig. 5.21 (b).

Further study deals with the investigation of temperature-dependent ac conductivity spectra of blend specimens of PPEL and nano-filler based PPELA series as plotted in Figs. 5.22 (a) and 5.23 (a), respectively. In case of PPEL series, at different $LiCF_3SO_3$ salt concentrations, the respective ac conductivity spectra show presence of single relaxation feature as also observed from Fig. 5.22 (b). On the other hand, at the initial concentration of Al_2O_3 nano-filler of 2 wt% in the blend of PPELA series, the ac conductivity spectra show presence of single relaxation feature at almost all temperatures. Interestingly, with further

addition of Al_2O_3 upto 6 wt%, the double relaxation feature starts persisting in the ac conductivity spectra even at higher temperatures.

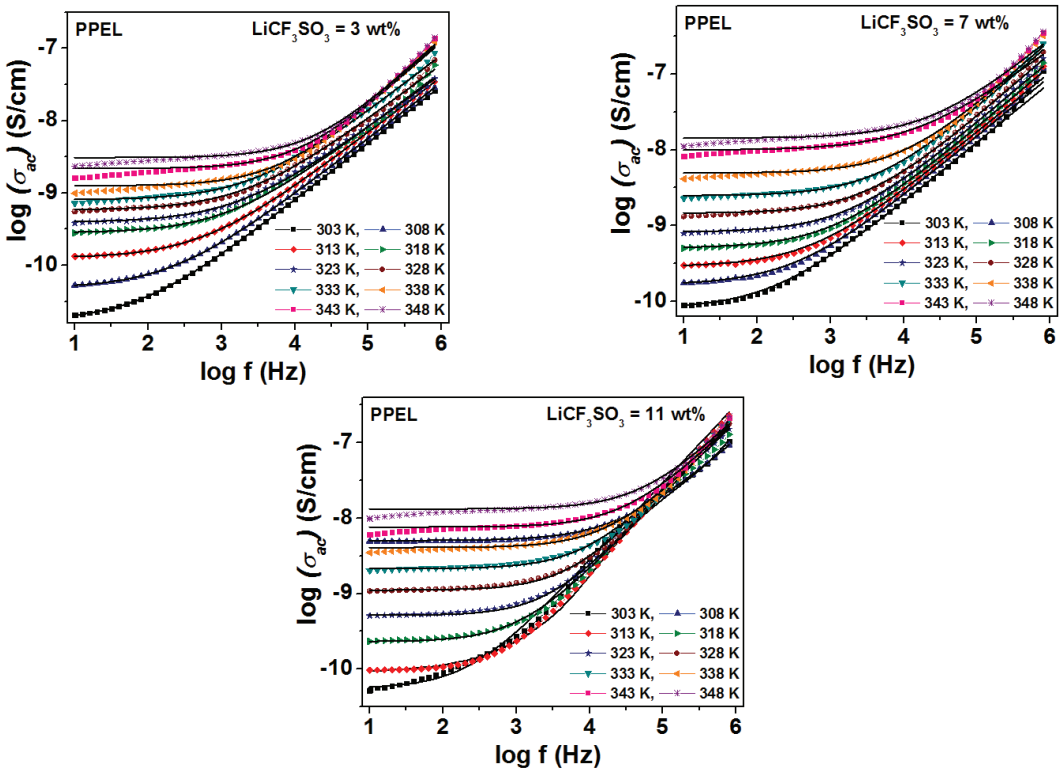

Fig. 5.22 (a) ac conductivity plots of blend specimens of PPEL series at different temperatures

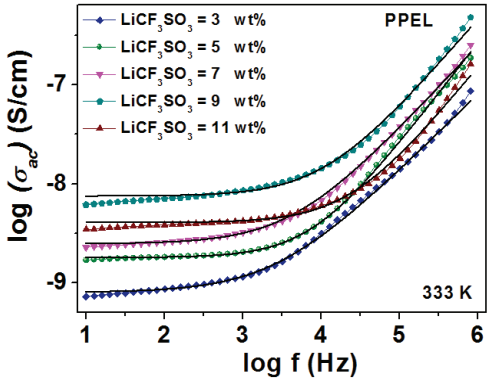

Fig. 5.22 (b) ac conductivity spectrum of blends of PPEL series at different $LiCF_3SO_3$ concentrations at 333 K

In this case, the two relaxations appear in ac conductivity spectra, because of the inhomogeneity in the polymer matrix. With further addition of Al_2O_3 nano-filler in blends upto 10 wt%, again single relaxation feature is observed in the respective ac conductivity

spectra. This is also clearly visible from Fig. 5.23 (b). However, as observed from each ac conductivity spectrum of Figs. 5.21 (a), 5.22 (a) and 5.23 (a), the dispersion frequency shifts towards higher frequency side with increasing temperature.

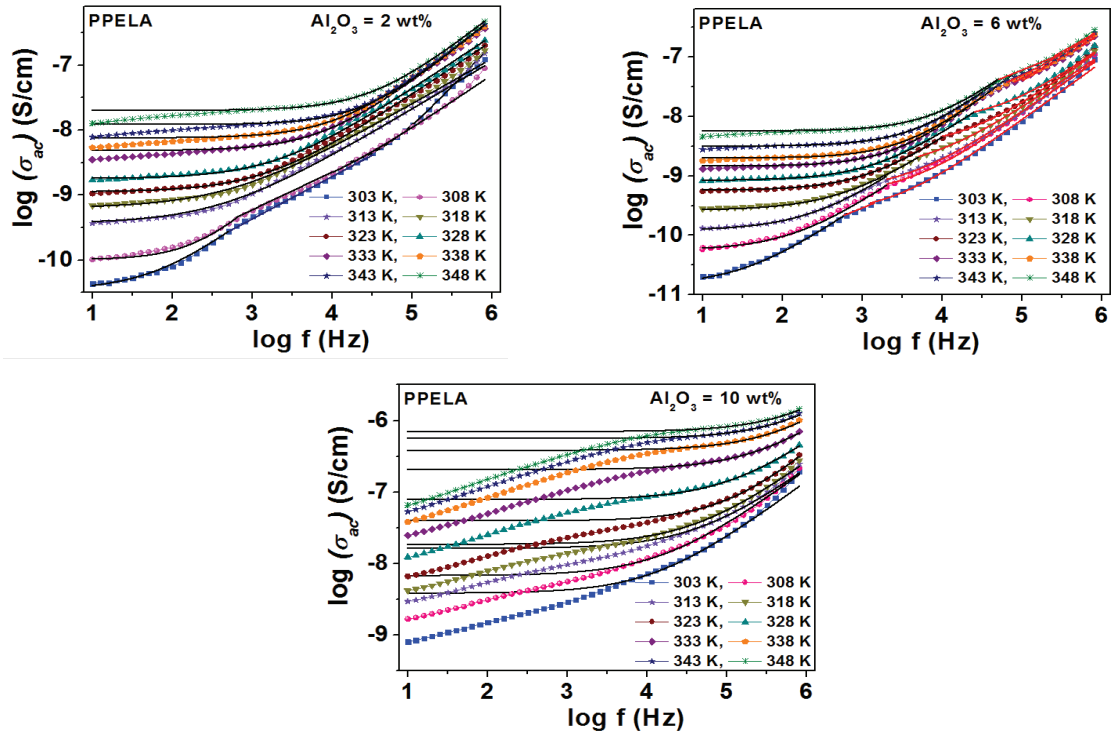

Fig. 5.23 (a) ac conductivity plots of blend specimens of PPELA series at different temperatures

But as seen from Fig. 5.21 (b), the dispersion frequency of ac conductivity spectra plotted at 333 K for various EC content with respect to logarithmic frequency (log f), shifts towards higher frequency side with gradual addition of EC in blends. But at EC > 6 wt%, this dispersion frequency shifts towards opposite side.

Further, as seen from Fig. 5.22 (b), wherein; ac conductivity data are plotted with respect to logarithmic frequency (log f) at 333 K for various $LiCF_3SO_3$ concentrations, the dispersion frequency shifts gradually towards higher frequency side with increasing $LiCF_3SO_3$ salt concentration upto 9 wt%. But with further addition of salt in PVA-PEO blend, this dispersion frequency shifts in the reverse direction.

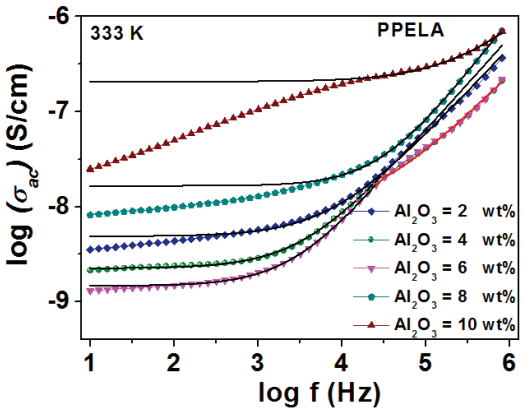

Fig. 5.23 (b) ac conductivity spectrum of blends of PPELA series at different Al_2O_3 concentrations at 333 K

Finally, in Fig. 5.23 (b), ac conductivity data are plotted at 333 K with respect to logarithmic frequency (log f) for various Al_2O_3 compositions. Interestingly, as seen from the figure, dispersion frequency initially shifts towards lower frequency side with addition of Al_2O_3 nano-filler in blends upto 6 wt%; but at Al_2O_3 > 6 wt%, this dispersion frequency is observed to shift towards higher frequency side.

5.2.3 *ac Conductivity Scaling*

Further, temperature-wise scaling of all these ac conductivity spectra of respective blend specimens with varying concentrations of EC plasticizer, lithium ($LiCF_3SO_3$) salt and Al_2O_3 nano-filler is carried out using Almond-West Formalism and shown in Figs. 5.24 (a), (b) and (c), respectively. As observed from Fig. 5.24 (a), at different concentrations of EC plasticizer, the respectively, temperature-wise scaled ac conductivity plot shows presence of a hump in the mid frequency region (beyond dispersion frequency). Moreover, at the high frequency regions also, these ac conductivity curves are seen to remain unmerged upto a maximum extent.

On the other hand, in the Fig. 5.24 (b) where the concentration of Li^+ salt is varied, ac conductivity spectra scaled at different temperatures show perfect overlapping but only from

low frequency regions upto dispersion frequency. Beyond dispersion frequency, ac conductivity curves do not superimpose perfectly to yield a single master curve.

Likewise PPEL series, the temperature-wise scaled ac conductivity spectra for blend specimens of PPELA series at initial concentrations of Al_2O_3 nano-filler also show perfect overlapping as depicted in Fig. 5.24 (c), but only from low frequency region upto dispersion frequency. Beyond dispersion frequency, these ac conductivity curves remain well-separated. However, with further addition of Al_2O_3 > 6 wt%, ac conductivity curves show perfect overlapping but from dispersion frequency to high frequency region. Below dispersion frequency, these curves remain well separated.

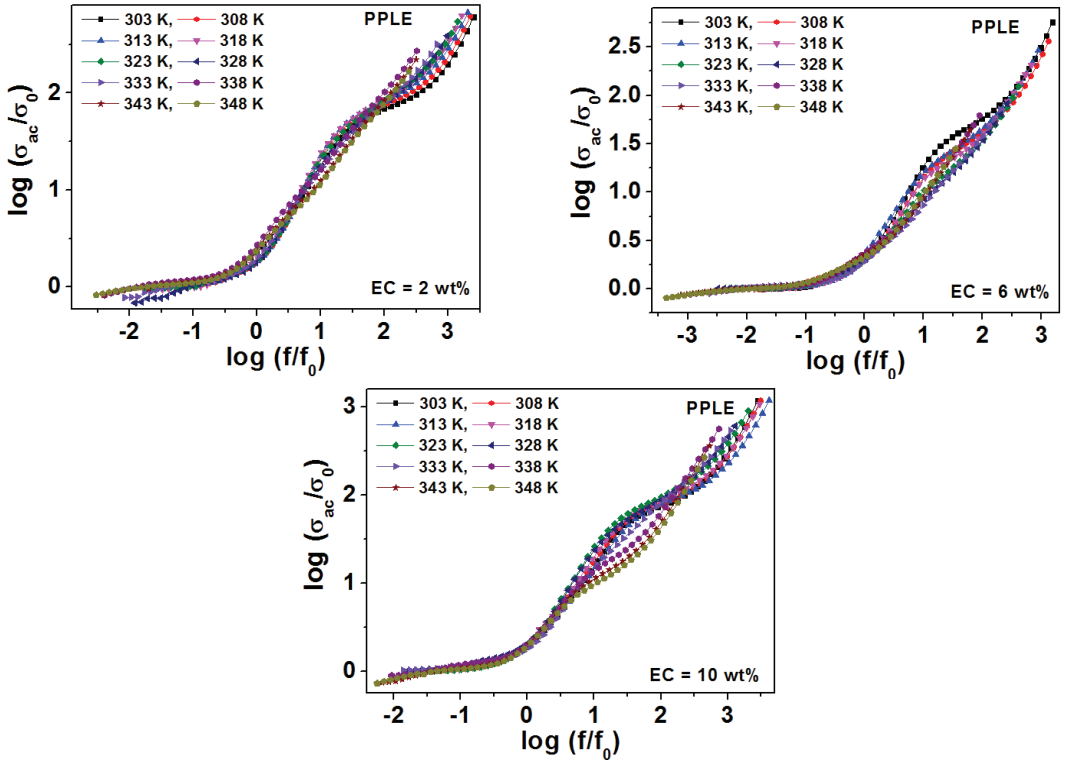

Fig. 5.24 (a) Scaling of ac conductivity spectra of blend specimens of PPLE series at different temperatures

Hence, for none of the blend specimens of PPLE, PPEL or PPELA series, temperature dependent ac conductivity data of respective ac conductivity spectrum coalesce into a single master curve. This suggests that ion dynamics in none of the blend specimens of respective Li^+ conducting series follow same mechanism throughout the temperature range.

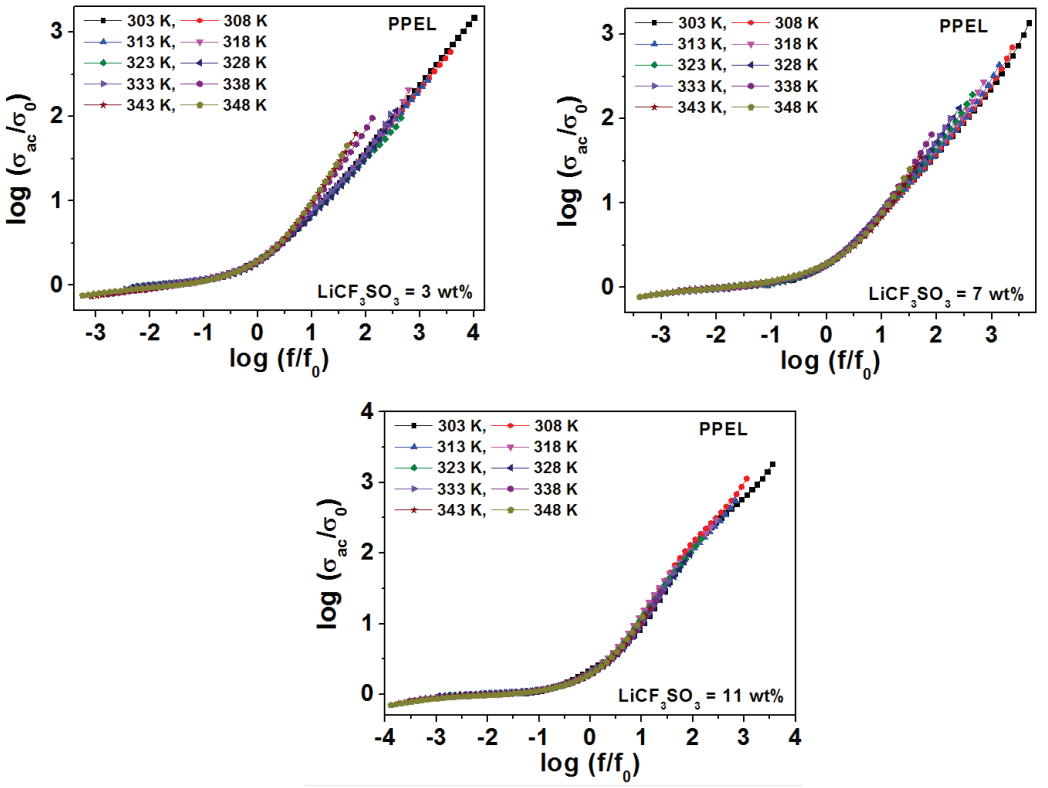

Fig. 5.24 (b) Scaling of ac conductivity spectra of blend specimens of PPEL series at different temperatures

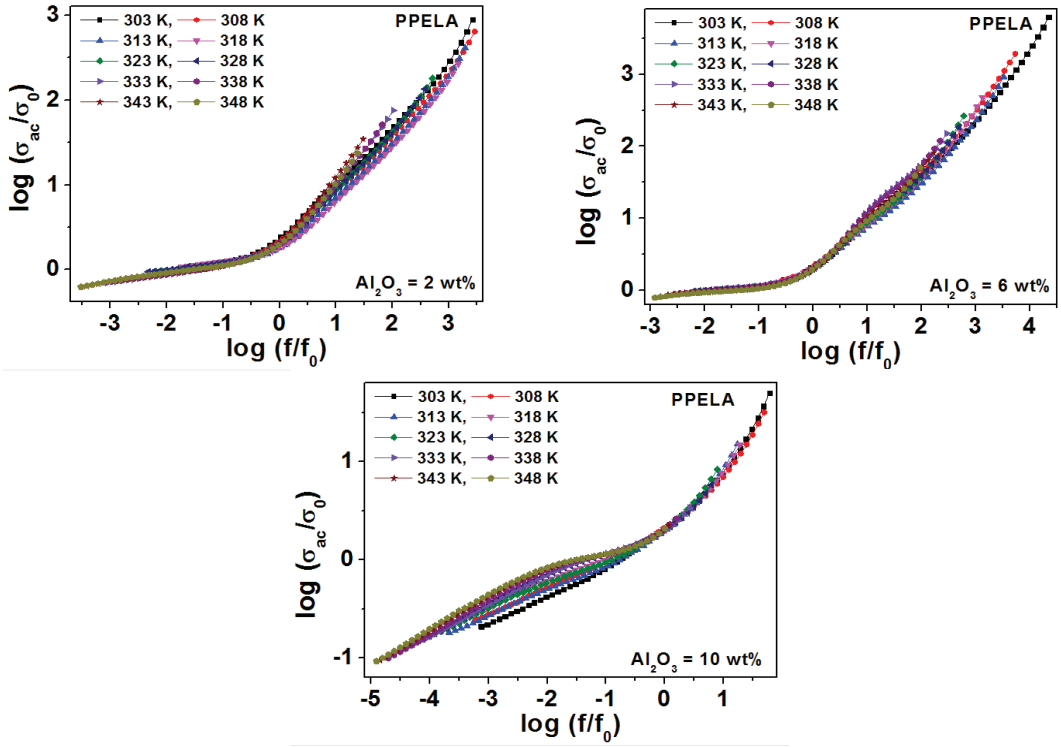

Fig. 5.24 (c) Scaling of ac conductivity spectra of blend specimens of PPELA series at different temperatures

Thus, *'Time-Temperature Superimposition Principle'* does not hold true for any of the blend specimens of Li^+ conducting series. This further indicates that in every respective blend specimen of PPLE, PPEL and PPELA series, Li^+ experience different environments to relax.

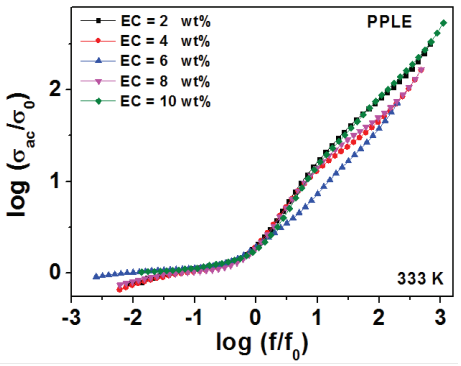

Fig. 5.25 (a) Scaling of ac conductivity spectrum of blends of PPLE series at different EC concentrations at 333 K

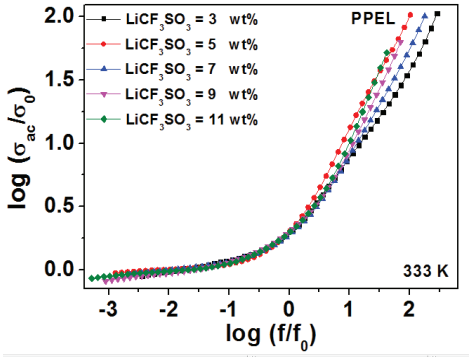

Fig. 5.25 (b) Scaling of ac conductivity spectrum of blends of PPEL series at different $LiCF_3SO_3$ concentrations at 333 K

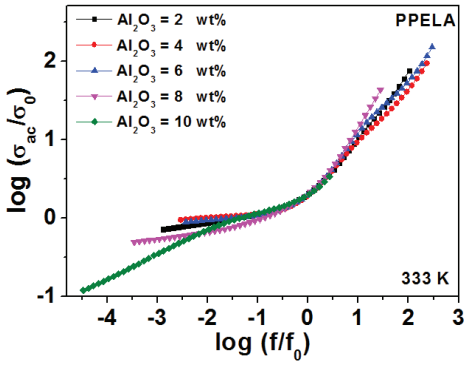

Fig. 5.25 (c) Scaling of ac conductivity spectrum of blends of PPELA series at different Al_2O_3 concentrations at 333 K

Also, concentration-wise scaling of ac conductivity spectra for different EC, $LiCF_3SO_3$ and Al_2O_3 concentrations is carried out at 333 K and demonstrated in the Figs. 5.25 (a), (b) and (c), respectively. As seen from Fig. 5.25 (a), ac conductivity curves for various EC concentrations get perfectly merged but only at dispersion region. However, below as well as beyond this dispersion frequency, these ac conductivity curves remain well-separated. Similar feature is also observed in case of blends of PPELA series as seen from Fig. 5.25 (c).

However, as seen from Fig. 5.25 (b), ac conductivity curves for different contents of $LiCF_3SO_3$ salt perfectly coalesce from low frequency region till dispersion frequency.

However, beyond dispersion frequency, each ac conductivity curve remains well-separated. This suggests that in case of blends of PPEL series, ion dynamics differ slightly, but at high frequency region. Otherwise, it follows *'Time-Concentration Superimposition Principle'*. In rest of the cases of PPLE and PPELA series, this principle is obeyed in dispersion frequency region. This suggests that no Li^+ conducting blend series thoroughly obeys the principle.

5.2.4 *dc Conductivity Studies*

Variation in the logarithmic values of dc conductivity 'log σ_{dc}' of the blends of PPLE, PPEL and PPELA series as a function of inverse of temperature have been depicted in Figs. 5.26 (a), (b) and (c), respectively. Here, these 'σ_{dc}' values are obtained by fitting the ac conductivity 'σ_{ac}' spectra of respective Li^+ conducting blends by using Jonscher's Power law (JPL) formula given in Eq. 5.4. As observed from each figure corresponding to respective PPLE, PPEL and PPELA series, the logarithmic values of dc conductivity 'log σ_{dc}' enhance systematically with the rising temperature. Conductivity of blend specimens with varying amount of EC of PPLE series enhances non-linearly with rising temperature and follows Vogel-Tamman-Fulcher (VTF) equation given as:

$$\sigma_{dc} = \sigma_0 T^{-1/2} \exp\left(\frac{-E_v}{k_B(T - T_0)}\right) \quad \ldots\ldots\ldots\ldots\ldots (5.8)$$

Similar behaviour is also observed for blend specimens of PPEL series wherein, the amount of $LiCF_3SO_3$ salt is varied. But in PPELA systems wherein, the concentrations of Al_2O_3 nano-filler is varied, conductivity shows non-linear i.e. VTF behaviour with respect to temperature for all the nano-composite blend specimens, except for the one with the highest Al_2O_3 content of 10 wt%. For this specimen with 10 wt% of Al_2O_3, conductivity obeys Arrhenius nature. Such an improvement in these 'log σ_{dc}' values with increasing temperature can be explained on the basis of *'Free Volume Theory'* [30-33]. Further, variation in logarithmic dc conductivity values 'log σ_{dc}' with respect to EC composition is shown in the

Fig. 5.27 (a). Here, upto 6 wt% of EC in PVA-PEO blends, conductivity enhances systematically as EC improves the amorphous phase in the blend matrix and gradually makes the blend system flexible. Hence, the conduction or migration of cations takes place effortlessly through this amorphous and flexible blend matrix. But with further addition of EC beyond 6 wt%, conductivity decreases substantially. This is possibly due to the formation of neutral aggregates of $LiCF_3SO_3$ salt with increasing content of EC in blends, which in turn block the conducting pathways and restrict the mobility of free Li^+ and $CF_3SO_3^-$ along with that of polymeric chain segments through the blend matrix.

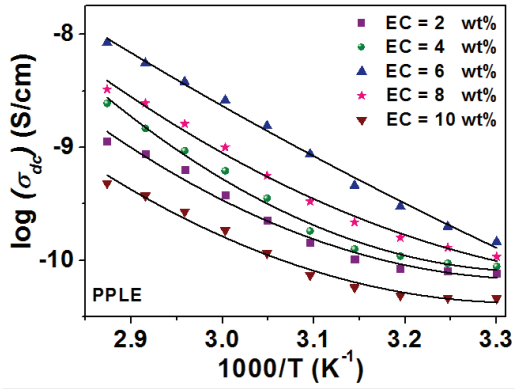

Fig. 5.26 (a) log σ_{dc} vs. 1000/T plot of blends of PPLE series

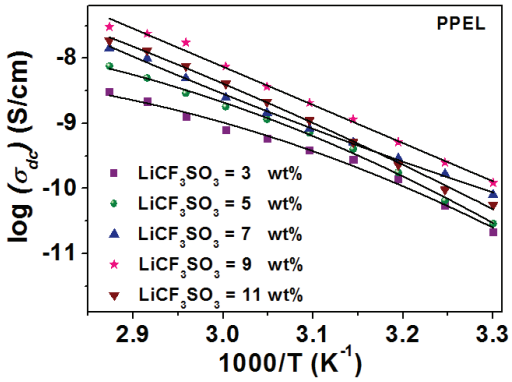

Fig. 5.26 (b) log σ_{dc} vs. 1000/T plot of blends of PPEL series

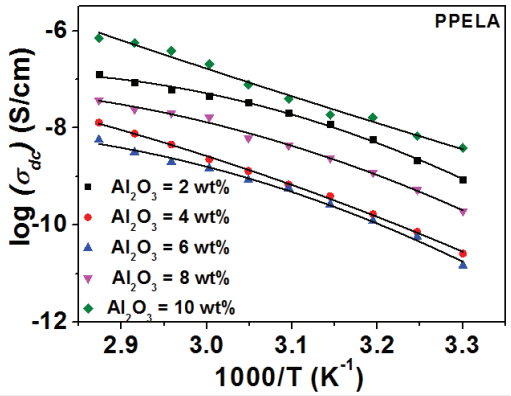

Fig. 5.26 (c) log σ_{dc} vs. 1000/T plot of blends of PPELA series

On the other hand, when $LiCF_3SO_3$ salt concentration in the blends of PPEL series is varied, conductivity rises slowly till 9 wt% of salt but beyond that, it slightly decreases, as seen from Fig. 5.27 (b). Here, with initial addition of salt, the process of salt dissociation to

form free charge carriers also enhances. Thus, the number of Li^+ participating in the conduction process and yielding dc conductivity also increases. This hence, leads to gradual enhancement of dc conductivity with addition of salt upto 9 wt%. But at 11 wt% of salt, these free charge carriers come closer to each other to form neutral aggregates. This process not only reduces the number of cations participating in the conduction process but also blocks the conduction pathways hence, restricting the movement of remaining free cations to participate in the process of conduction. All these factors in turn drop the dc conductivity at 11 wt% of salt concentration.

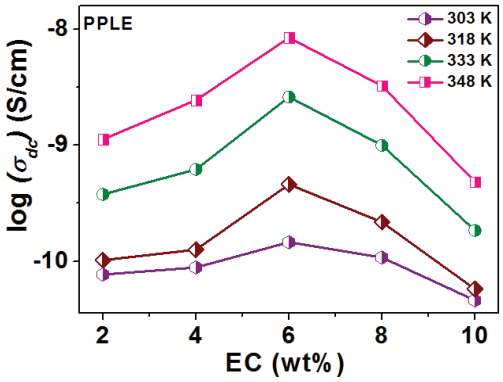

Fig. 5.27 (a) log σ_{dc} vs. EC concentrations

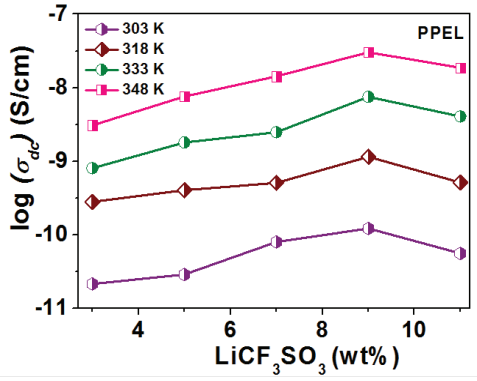

Fig. 5.27 (b) log σ_{dc} vs. $LiCF_3SO_3$ concentrations

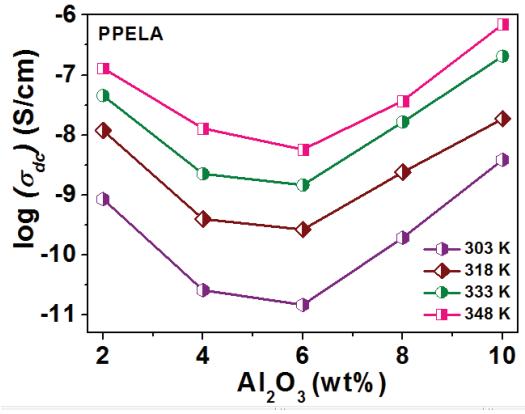

Fig. 5.27 (c) log σ_{dc} vs. Al_2O_3 concentrations

Finally, with incorporation of Al_2O_3 nano-filler in the blends of PPELA series, logarithmic dc conductivity 'log σ_{dc}' is observed to firstly reduce substantially. However, beyond 6 wt% of Al_2O_3 in blends, 'log σ_{dc}' significantly enhances as seen from Fig. 5.27 (c).

Such a variation in dc conductivity with respect to Al_2O_3 concentration as depicted by Li^+ conducting PPELA series is completely reverse to that observed for Ag^+ conducting PPAPA series. When Al_2O_3 nano-filler is added at initial levels in the blends of PPELA series, instead of facilitating amorphous phases and free volume in blend matrix, the nano-filler particles come together and form neutral aggregates which in turn not only block the conducing pathways but also increase the crystallinity of blend matrices thus, reducing its flexibility. All these factors in turn reduce mobility of free Li^+ and $CF_3SO_3^-$ as well as polymer chain segments through blend matrices and result in the drop of dc conductivity with increasing content of Al_2O_3 nano-filler in blends. However, at the higher concentrations of Al_2O_3 beyond 6 wt%, random distribution of nano-filler particles initiates the formation of free volume in blend matrix. This increases amorphicity of the blend matrix, imparts flexibility to it and avails conducting pathways for the transport of free Li^+ and $CF_3SO_3^-$ and segments of polymer chains through it. Owing to all these factors, '$\log \sigma_{dc}$' values enhance significantly at Al_2O_3 > 6 wt% in the blends of PPELA series. Hence, the nano-composite blend specimen with 10 wt% of Al_2O_3 nano-filler depicts optimum dc conductivity value than the rest of the blends of PPELA series. **Weston et al.** [73] and **Joge et al.** [74] also reported the similar observation with respect to Al_2O_3 concentrations in their respective nanocomposite $LiClO_4$-PEO-α-alumina and PVA-PEO-EC-$LiCF_3SO_3$-Al_2O_3 systems.

5.2.5 ***Conduction Hopping Frequency***

For each temperature, fitting of ac conductivity data of every respective Li^+ conducting blend specimen is done by using Jonscher's Power Law (JPL) equation to obtain the respective values of power law exponent 'n' and constant 'A'. By substituting these respective values of 'n' and 'A' along with those dc conductivity 'σ_{dc}' in Eq. 5.5, the values of conduction hopping frequency 'ω_h' are respectively obtained for each respective Li^+ conducting blend specimen at all the temperatures. Variation in the logarithmic values of

conduction hopping frequency 'log ω_h' with inverse of temperature for each respective blend specimen of PPLE, PPEL and PPELA series is depicted in Figs. 5.28 (a), (b) and (c), respectively. As observed from each figure, 'log ω_h' values increase linearly with rising temperature following the Arrhenius relation which suggests that conduction hopping frequency is a thermally activated process.

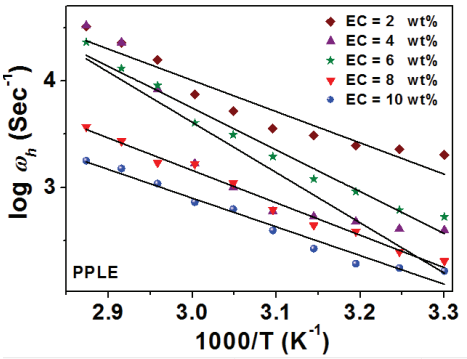

Fig. 5.28 (a) log ω_h vs. 1000/T plot of blends of PPLE series

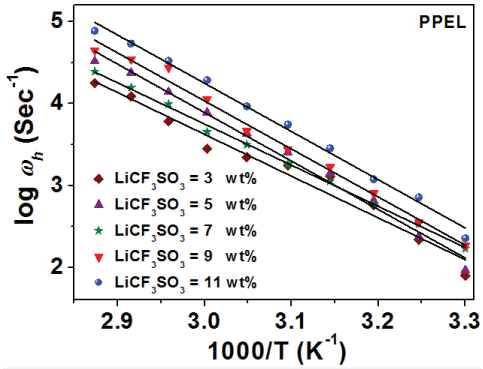

Fig. 5.28 (b) log ω_h vs. 1000/T plot of blends of PPEL series

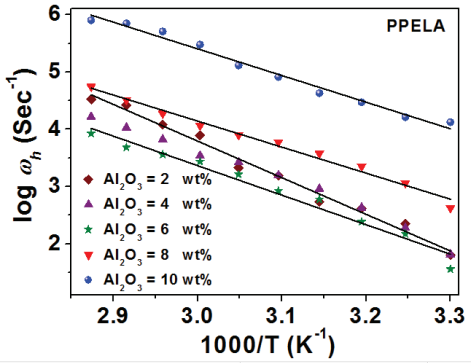

Fig. 5.28 (c) log ω_h vs. 1000/T plot of blends of PPELA series

5.2.6 ***Modulus Studies***

In order to understand relaxation dynamics of blends of Li^+ conducting PPLE, PPEL and PPELA series, their electric modulus is investigated. Fig. 5.29 (a) depicts the variation in imaginary parts of modulus (M") with respect to logarithmic values of frequency (log f) of blend specimens of PPLE series at different temperatures in the range of 303 K to 348 K.

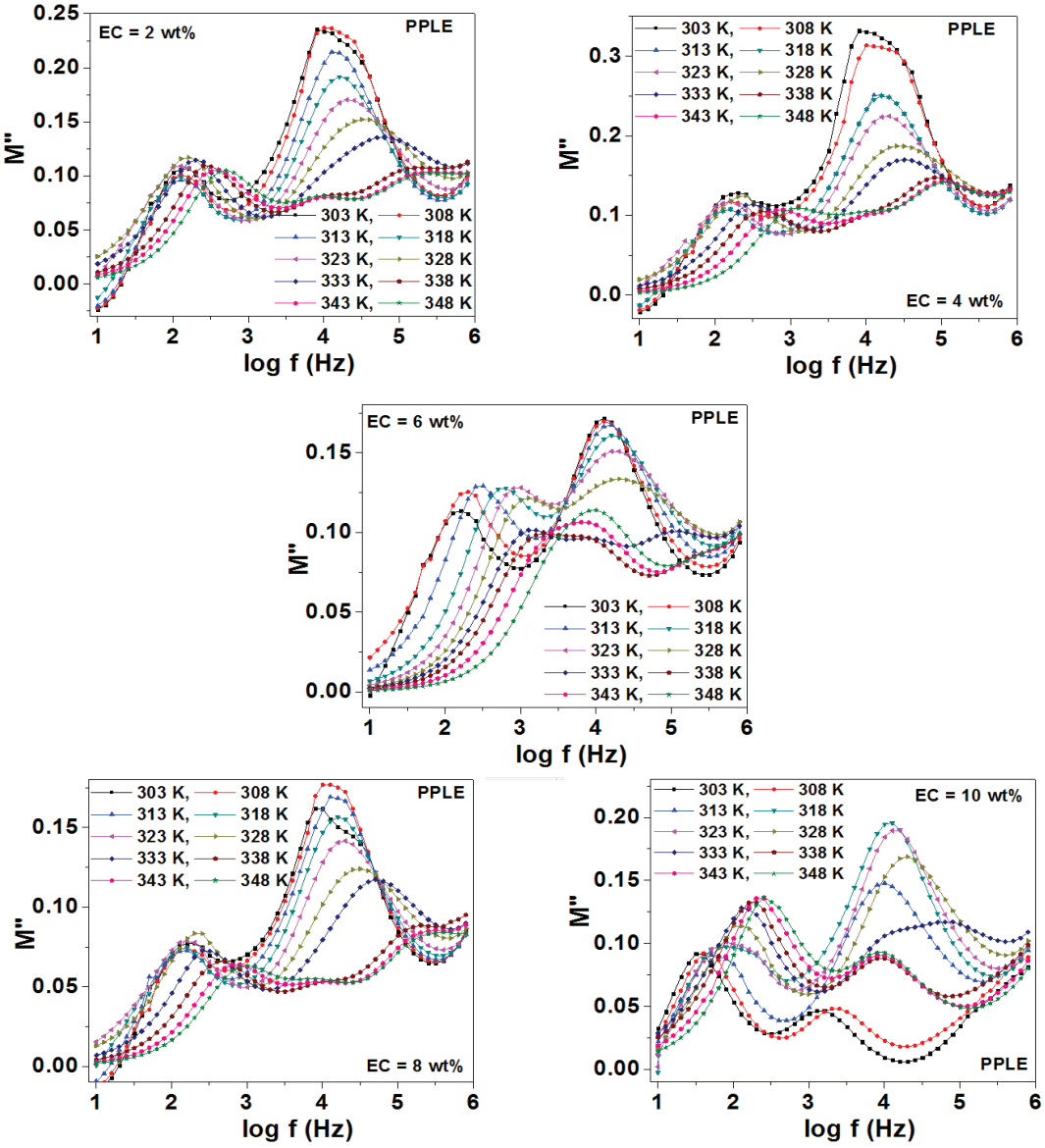

Fig. 5.29 (a) Modulus spectra of blend specimens of PPLE series at different temperatures

Likewise ac conductivity spectra, modulus spectra of respective blend specimens of PPLE series also show presence of a double relaxation peak feature. Here, maxima of the first relaxation peak lies in low-mid frequency region whereas; that of second relaxation peak exists at mid-high frequency region. Such a double relaxation feature is also observed by **Sharma et al.** [72] for their EC plasticized PEO-PMMA-$AgNO_3$ blend system. The two relaxation peaks in the present cases may be assigned to the respective conductivity

processes. At low-mid frequencies, the conduction relaxation processes are observed whereas; the mid-high frequencies are assigned to the segmental one.

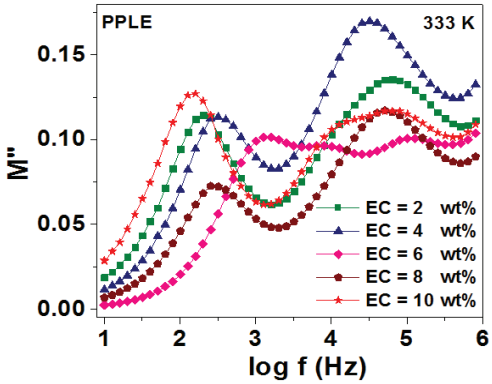

Fig. 5.29 (b) Modulus spectrum of blends of PPLE series at different EC concentrations at 333 K

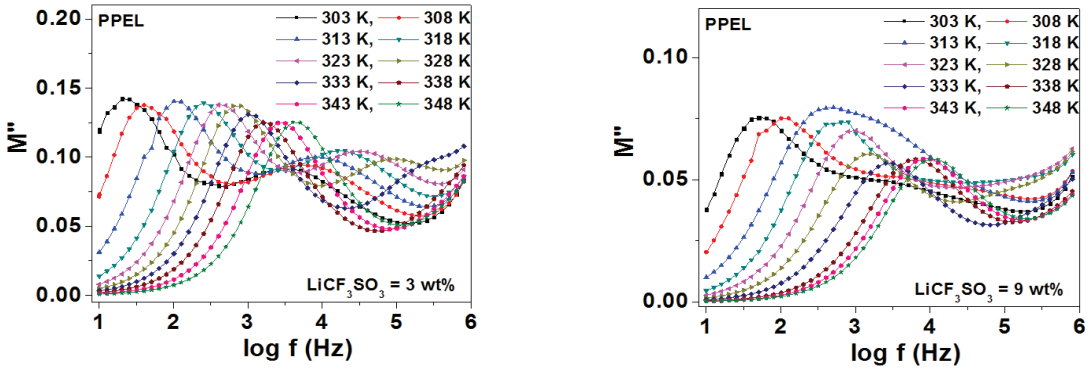

Fig. 5.30 (a) Modulus spectra of blend specimens of PPEL series at different temperatures

Further, as shown in Fig. 5.29 (a), for the blends with 2 wt%, 4 wt% and 8 wt% of EC, the second relaxation peak appearing at mid-high frequency region is observed to shift gradually towards higher frequency side with rising temperature. However, the position of first conduction relaxation peak existing at low-mid frequency region hardly changes with temperature. On the contrary, for the blends with 6 wt% and 10 wt% of EC, the first relaxation peak shifts towards higher frequency side with increasing temperature whereas; the shift/change in the position of second relaxation peak is very small with respect to temperature rise. Interestingly, the low-mid frequency relaxation peak appearing in the modulus spectrum as depicted in Fig. 5.29 (b), initially shifts towards higher frequencies with

increasing amount of EC in blends upto 6 wt%. But with further incorporation of plasticizer in blends, this relaxation peak shifts back to the lower frequency side. However, the relaxation peak appearing in the mid-high frequency side shifts randomly with the addition of EC in blends.

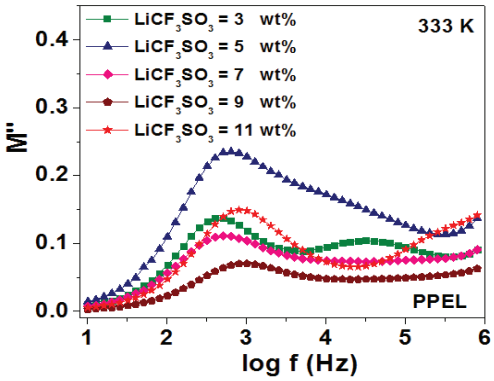

Fig. 5.30 (b) Modulus spectrum of blends of PPEL series at different $LiCF_3SO_3$ concentrations at 333 K

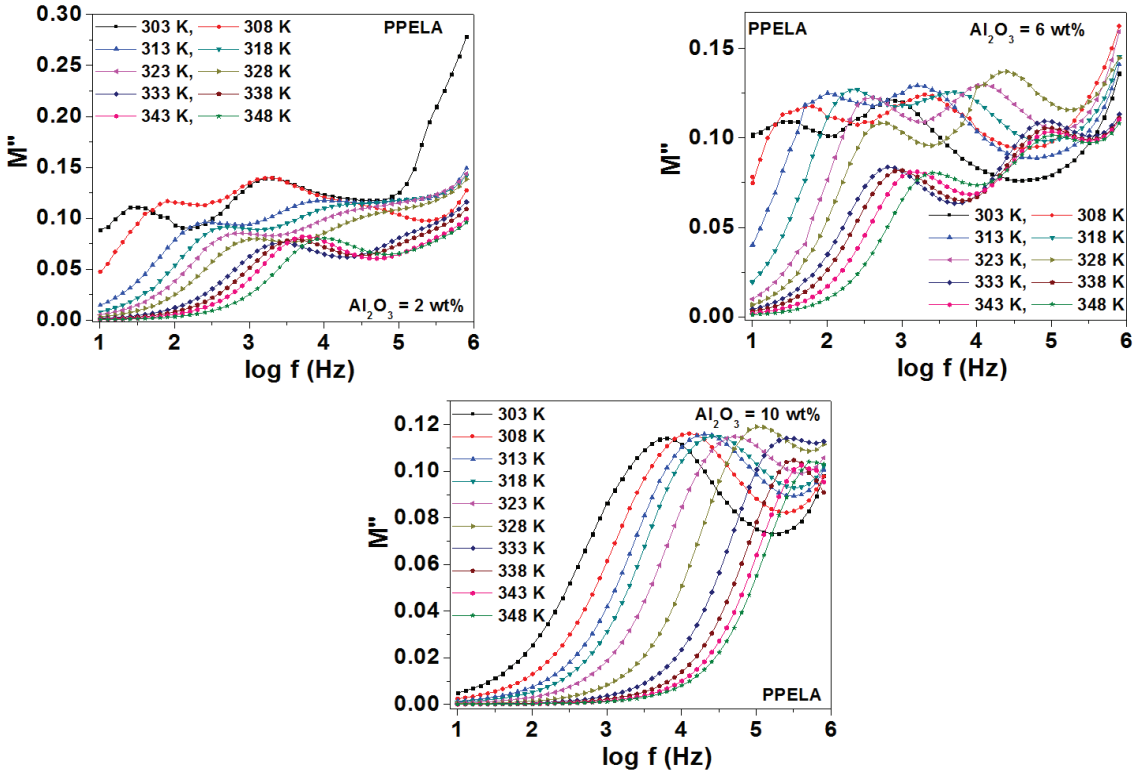

Fig. 5.31 (a) Modulus spectra of blend specimens of PPELA series at different temperatures

When $LiCF_3SO_3$ salt concentration is varied in the blends of PPEL series as shown in Fig. 5.30 (a), the low-mid frequency relaxation is dominant and the relaxation peak shifts

towards high frequency side as temperature increases. This suggests that the segmental relaxation is not very prominent in this blend series. However, as observed from Fig. 5.30 (b), the relaxation peak shifts randomly with the incorporation of $LiCF_3SO_3$ salt in the blends.

In the blend polymer electrolytes of PPELA series, when Al_2O_3 nano-filler is added at initial levels the M" vs. log f spectra as shown in Fig. 5.31 (a) show presence of two relaxation features occurring in low-mid and mid-high frequency regions at lower temperatures. But when temperature is raised, only single relaxation feature is observed at low-mid frequency region, suppressing the relaxation feature at mid-high frequencies occurring due to segmental motion in the blends. Hence, with the addition of Al_2O_3 nano-filler in PVA-PEO-EC-$LiCF_3SO_3$-Al_2O_3 series, the imaginary part of modulus (M") values plotted with respect to logarithmic frequency (log f) provide two conduction relaxations but only at lower temperatures. Exceptionally in case of the nano-composite blend with 10 wt% of Al_2O_3, only single relaxation peak is observed in its M" vs. log f spectra, in the entire temperature range. This relaxation peak shifts gradually towards higher frequency side with the rising temperature.

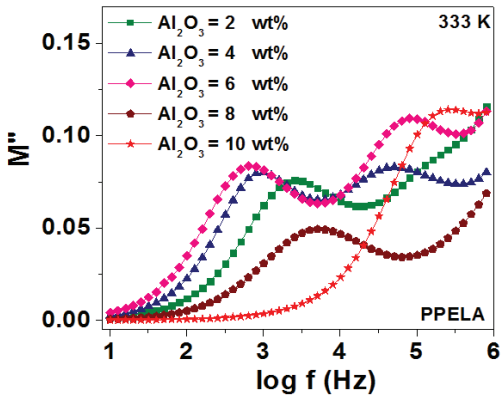

Fig. 5.31 (b) Modulus spectrum of blends of PPELA series at different Al_2O_3 concentrations at 333 K

Finally, as observed from the modulus spectra as shown in Fig. 5.31 (b), at lowest concentration of Al_2O_3 in blends, a single relaxation feature appears at low-mid frequency region. With further increase of nano-filler in blends, another peak at mid-high frequency

region gets its prominence. However, beyond 6 wt% of Al_2O_3, this peak gradually loses its prominence and disappears completely. Interestingly, the peak maxima appearing in low-mid frequency region shifts systematically towards low frequency side with the addition of Al_2O_3 upto 6 wt% in the blends whereas; with further addition of Al_2O_3, this peak maxima substantially shifts in the reverse direction.

5.2.7 ***Modulus Scaling***

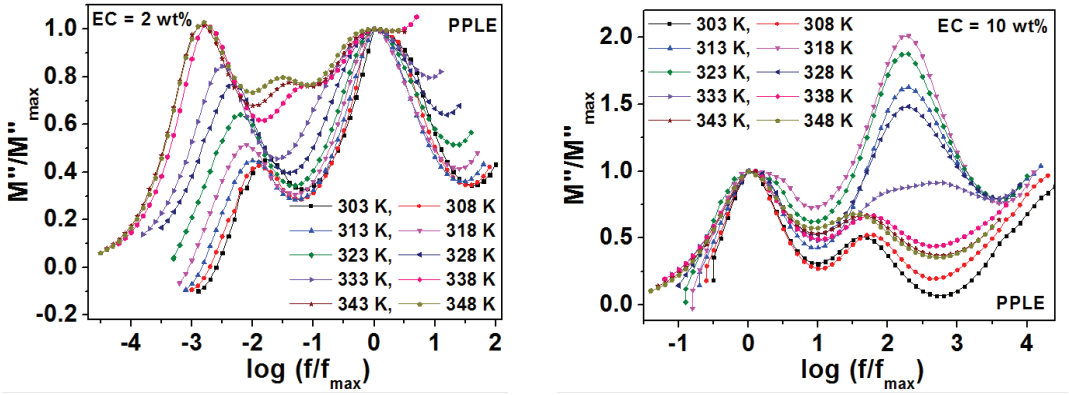

Fig. 5.32 (a) Scaling of modulus spectra of blend specimens of PPLE series at different temperatures

Further study deals with temperature-wise as well as concentration-wise scaling of modulus spectra of blends of all Li^+ conducting series. Figs. 5.32 (a), (b) and (c) show temperature-wise scaling of modulus spectra of blends wherein; EC, $LiCF_3SO_3$ and Al_2O_3 concentrations are respectively, varied. As observed from each figure, for Li^+ conducting specimen of PPLE, PPEL or PPELA series, none of the modulus spectra coalesce perfectly to yield a single master curve. This suggests that likewise the ion dynamics for conduction process, the relaxation dynamics also majorly depends upon temperature and does not follow *'Time-Temperature Superimposition Principle'*.

Moreover, concentration-wise modulus scaling of blends of each of the Li^+ conducting PPLE, PPEL and PPELA series is being carried out at 333 K and depicted in Figs. 5.33 (a), (b) and (c), respectively. In each Li^+ conducting series, the modulus curves of the

respectively concentration-wise plotted modulus spectra are unable to coalesce perfectly to yield a single master curve. This suggests that likewise the ion dynamics for conduction, the relaxation dynamics also follow different mechanisms at various concentrations of EC plasticizer, $LiCF_3SO_3$ salt as well as Al_2O_3 nano-filler.

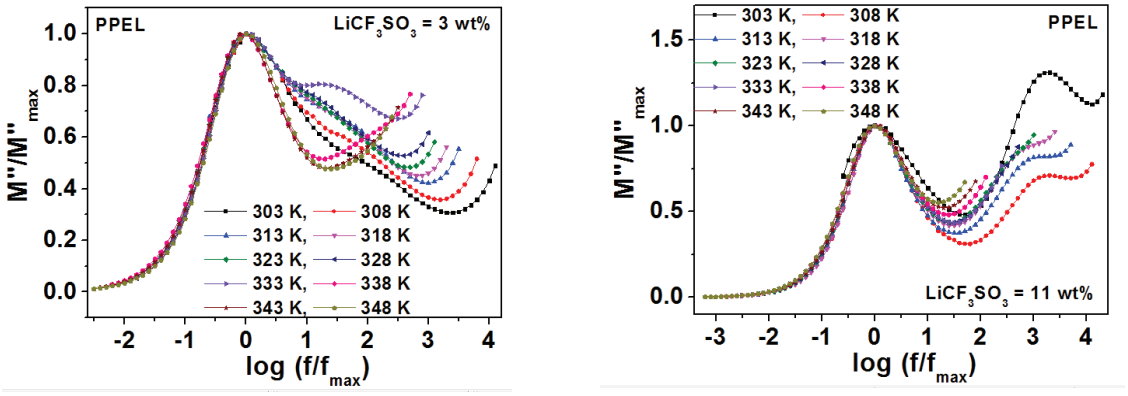

Fig. 5.32 (b) Scaling of modulus spectra of blend specimens of PPEL series at different temperatures

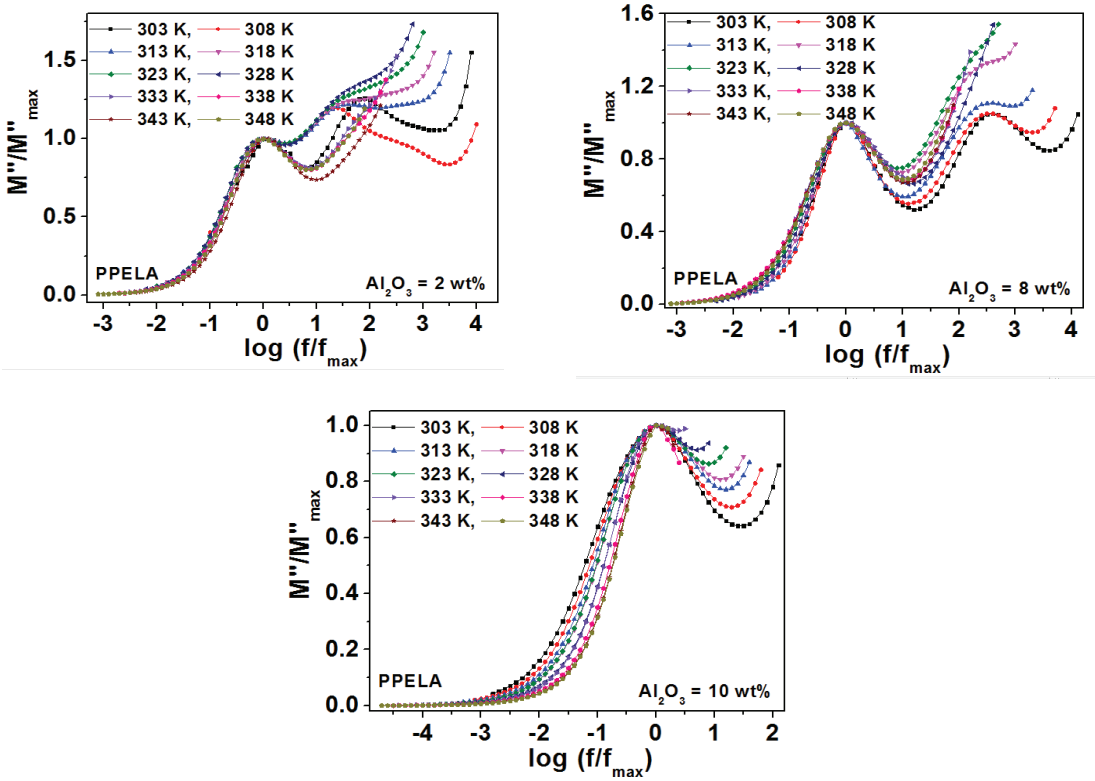

Fig. 5.32 (c) Scaling modulus spectra of blend specimens of PPELA series at different temperatures

Hence, the *Time-Concentration Superimposition Principle'* is not followed by any of the Li^+ conducting PPLE, PPEL or PPELA series. Similar features as seen in the present cases are also observed and discussed by **Gondaliya et al.** [42] in their poly(ethylene oxide)–silver triflate solid polymer electrolyte system.

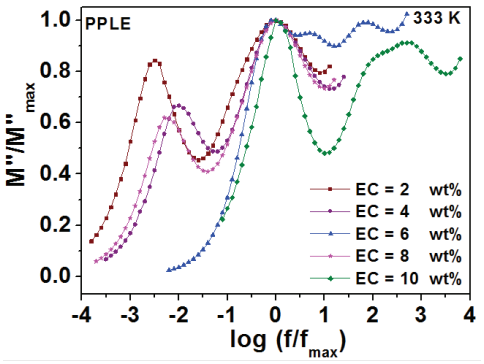

Fig. 5.33 (a) Scaling of modulus spectrum of blends of PPLE series at different EC concentrations at 333 K

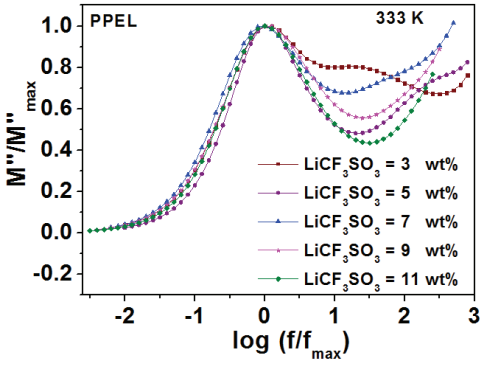

Fig. 5.33 (b) Scaling of modulus spectrum of blends of PPEL series at different $LiCF_3SO_3$ concentrations at 333 K

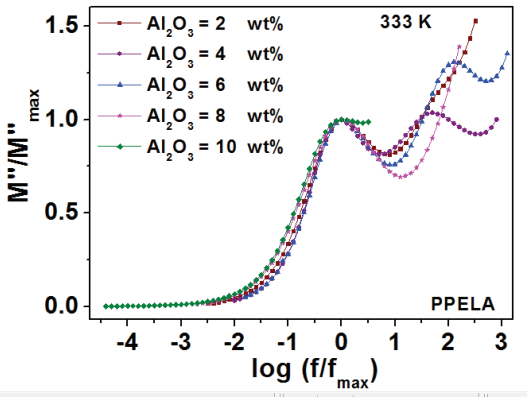

Fig. 5.33 (c) Scaling of modulus spectrum of blends of PPELA series at different Al_2O_3 concentrations at 333 K

5.2.8 ***Relaxation Time***

Values of maximum frequency 'f_{max}' corresponding to the peak maxima of the respective temperature-wise modulus spectra of the blends of each Li^+ conducting series are substituted in Eq. 5.6 to obtain the respective values of relaxation time 'τ'. Variation in logarithmic relaxation time (log τ) values corresponding to the respective blends of PPLE, PPEL and PPELA series is plotted with respect to inverse of temperature and shown in the

Figs. 5.34 (a), (b) and (c), respectively. The figures show a linear drop in the 'log τ' values with the rise in temperature and suggest that relaxation time follows Arrhenius rule. This Arrhenius variation of the 'log τ' values with respect to temperature also indicates that relaxation time is a thermally activated process [50-55].

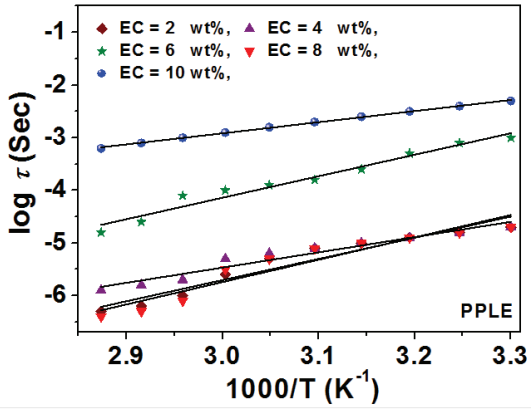

Fig. 5.34 (a) log τ vs. 1000/T plot of blends of PPLE series

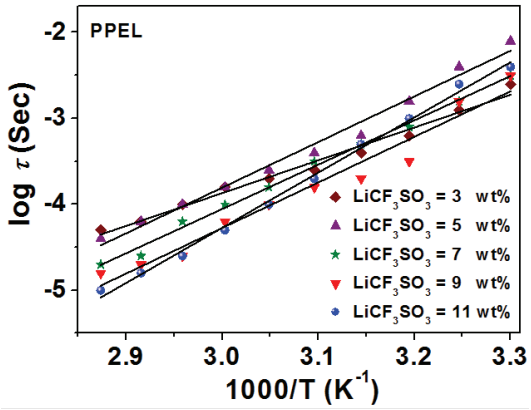

Fig. 5.34 (b) log τ vs. 1000/T plot of blends of PPEL series

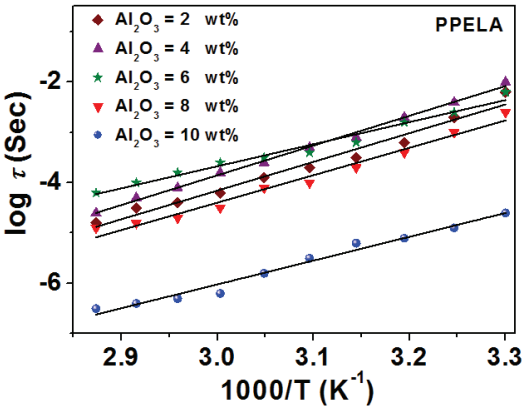

Fig. 5.34 (c) log τ vs. 1000/T plot of blends of PPELA series

5.2.9 ***Dielectric Studies***

In order to understand dielectric properties of blends of Li^+ conducting PPLE, PPEL and PPELA series, their dielectric parameters including dielectric constant (ε') and dielectric loss (ε") are investigated in details. Figs. 5.35 (a), (b) and (c) depict temperature-wise variation in dielectric constant (ε') with respect to logarithmic values of frequency (log f) of blends of PPLE, PPEL and PPELA series, respectively.

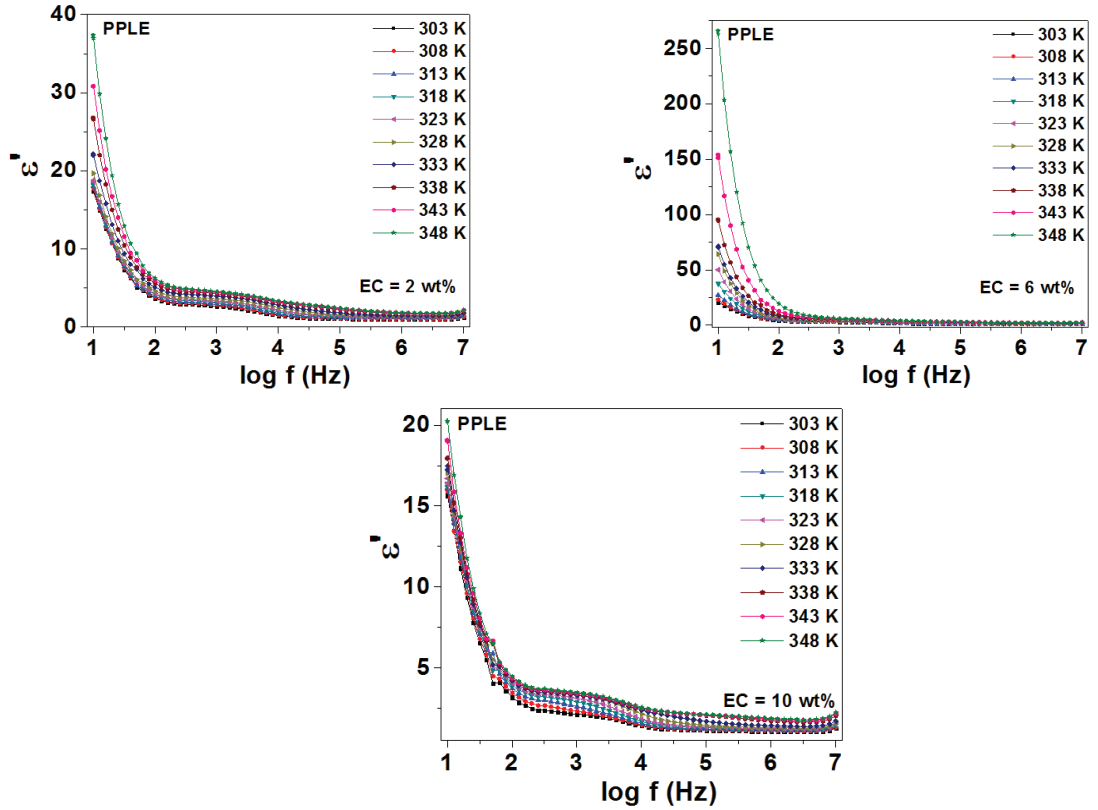

Fig. 5.35 (a) ε' vs. log f spectra of blend specimens of PPLE series at different temperatures

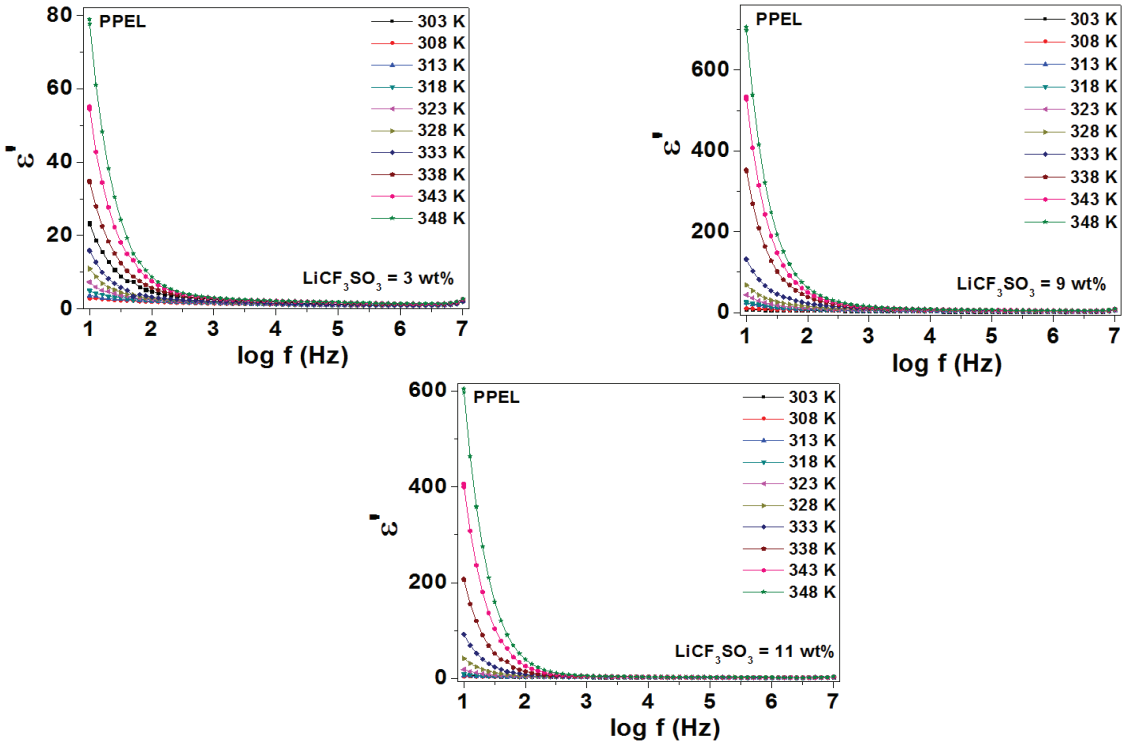

Fig. 5.35 (b) ε' vs. log f spectra of blend specimens of PPEL series at different temperatures

On the other hand, dielectric loss (ε") vs. logarithmic values of frequency (log f) plots of blends of PPLE, PPEL and PPELA series at different temperatures are shown in the Figs. 5.36 (a), (b) and (c), respectively. As observed from the respective figures, dielectric constant (ε') as well as dielectric loss (ε") values are found to be larger at lower frequencies. However, these ε' and ε" values drop gradually with increasing frequency and beyond dispersion frequency, they remain low and almost constant even with further increase in frequency. When frequencies are low, there is enough time available for the dipoles of polymeric macromolecules to orient themselves in the direction of applied electric field. Also, Li^+ can get immediately accumulated at electrode-electrolyte interfacial regions at lower frequencies [11,30,56,57]. Owing to this fact, the values of dielectric constant (ε') as well as dielectric loss (ε") are high at low frequencies.

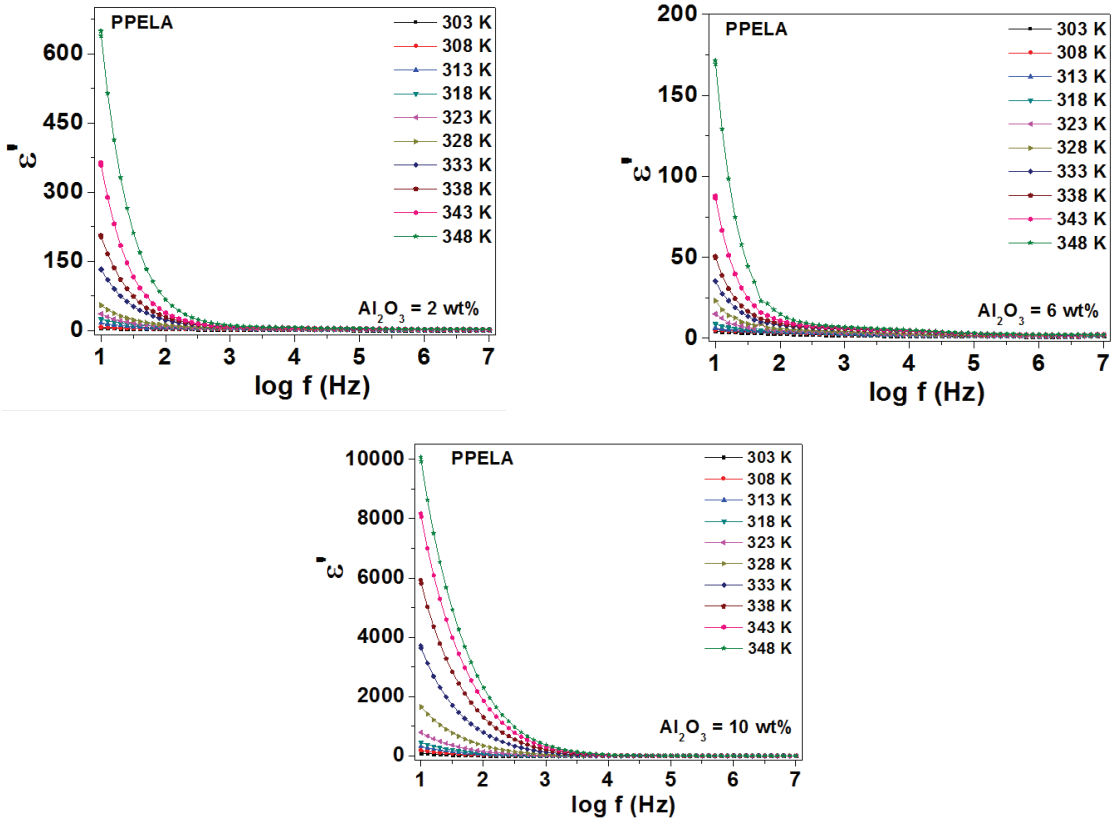

Fig. 5.35 (c) ε' vs. log f spectra of blend specimens of PPELA series at different temperatures

Hence, the electrode polarization and space charge effects are mainly responsible for consistent rise in the values of both dielectric constant (ε') as well as dielectric loss (ε") with reducing frequencies. Presence of such polarization effect also indicates the non-Debye type of behaviour [8]. On the other hand, as frequency increases, the polarity of applied electric field changes rapidly owing to which the dipoles of macromolecules start facing difficulty in coping with it. Moreover, migration of ions lowers down with the increasing frequency. All these factors lead to drop in ε' and ε" values as frequency increases. With further rise in frequency beyond dispersion frequency, the reversal of applied electric field gets so rapid that the dipoles of polymeric macromolecules are unable to orient themselves in the direction of this field. Moreover, diffusion of ions significantly mitigates at frequencies higher than dispersion frequency. These factors lead to low and constant values of dielectric constant (ε') as well as dielectric loss (ε") at frequencies beyond dispersion frequency [30,58,59].

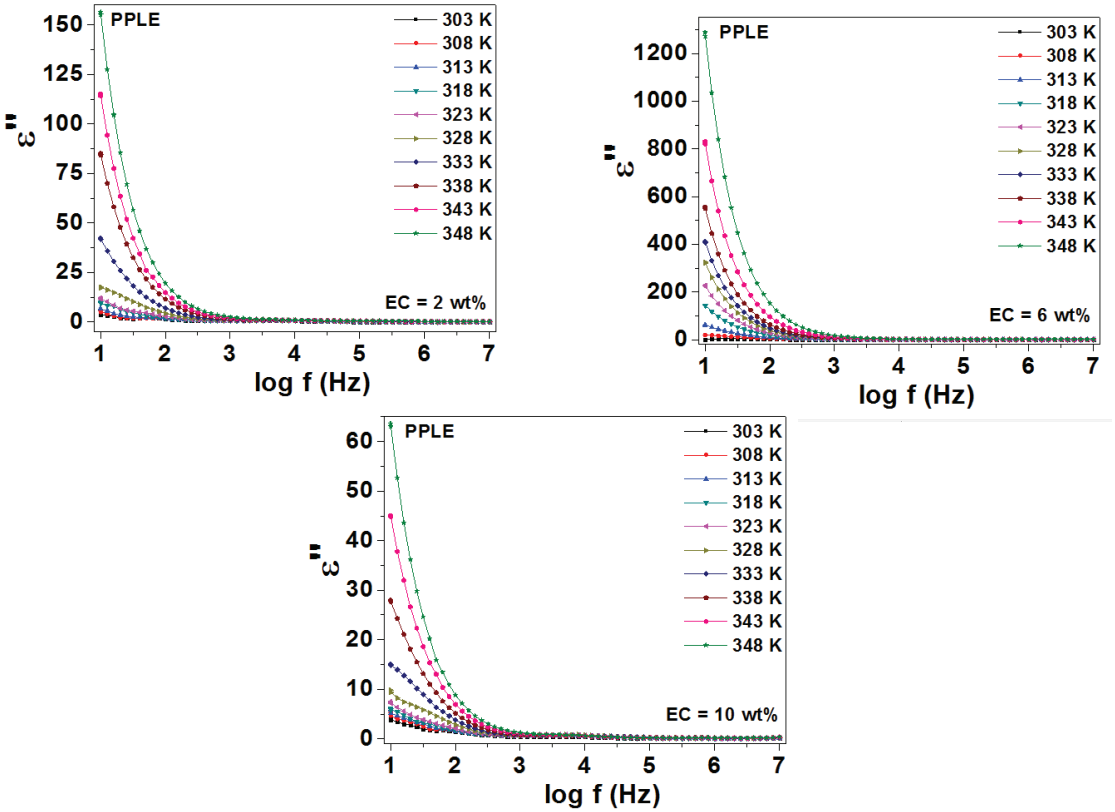

Fig. 5.36 (a) ε" vs. log f spectra of blend specimens of PPLE series at different temperatures

Further, at any particular frequency below dispersion frequency, values of both dielectric constant (ε') as well as dielectric loss (ε") are observed to enhance significantly with increasing temperature. This phenomenon can be assigned to the thermal activation of charge and energy requirement for transition of ions from one site to another. The direct measure of this energy dissipated is dielectric loss which contributes in the transport of ions and polarization of dipoles or charges. As temperature increases, these processes of orientation of dipoles of polymeric macromolecules as well as transport of free charge carriers also get significantly active. Thus, the amount of energy loss taking place in the occurrence of these processes also increases automatically. This in turn results in the enhancement of dielectric loss values with increasing temperature.

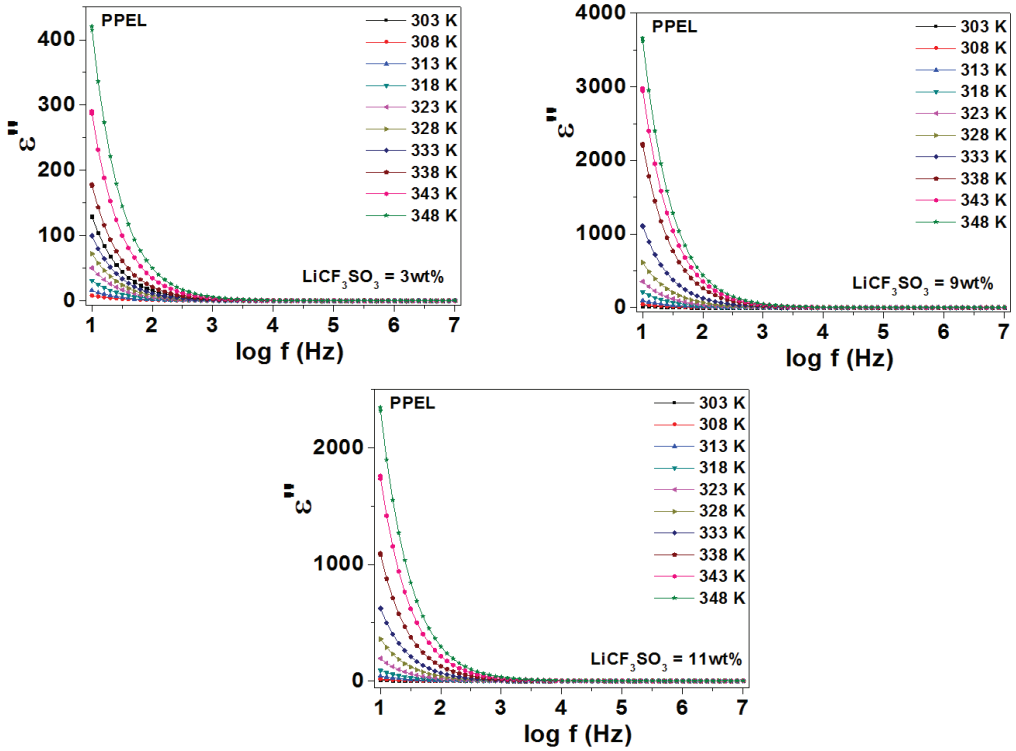

Fig. 5.36 (b) ε" vs. log f spectra of blend specimens of PPEL series at different temperatures

This suggests that the ion jumps and dc conduction losses in addition to polarization losses are the major contributors of high dielectric loss values with respect to temperature rise. It is highly interesting to see that all these processes occur successfully but only at

frequencies < dispersion frequency. At frequencies > dispersion frequency, quick reversal of electric field slows down all these processes. Additionally, the dispersion frequency in each dielectric spectrum is found to shift towards higher frequency side with increasing temperature. This is because as temperature increases, relaxation of polymer chain segments gets faster. This in turn promotes flexibility to the polymeric chain segments and hence, facilitates their motion through the polymer blend matrix. Moreover, the rise in temperature also enhances the mobility of free charge carriers through this matrix under the action of applied electric field. All these factors lead to the gradual shifting of dispersion frequency towards higher frequency side as temperature increases. However, no peak feature is observed in any of the dielectric constant or dielectric loss spectra which indicates the dominance of dc conductivity [57,60]. Also, at every particular frequency < dispersion frequency of each dielectric spectra, ε' and ε" values vary in the fashion similar to dc conductivity with respect to the EC, $LiCF_3SO_3$ and Al_2O_3 concentrations, respectively.

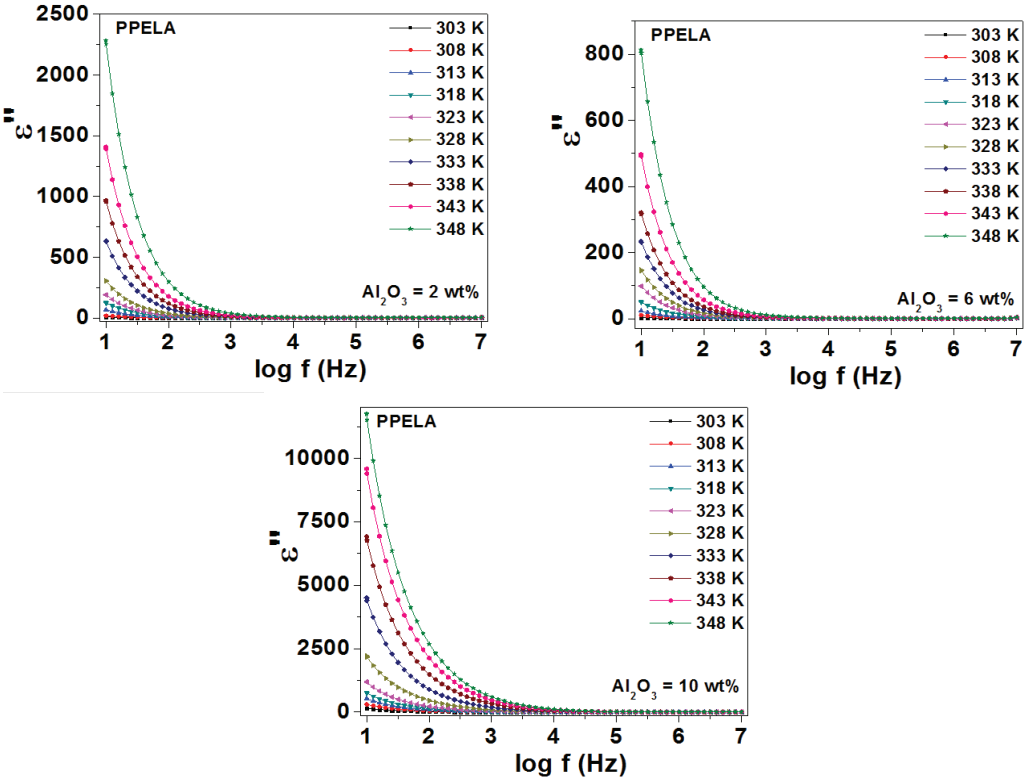

Fig. 5.36 (c) ε" vs. log f spectra of blend specimens of PPELA series at different temperatures

References

[1] R. Muchakayala, S. Song, S. Gao, X. Wang, Y. Fan, *Polymer Testing* 58 (2017) 116.

[2] P. Joge, D.K. Kanchan, P. Sharma, N. Gondaliya, *AIP Conf. Proc.* 1349 (2011) 1053.

[3] E. Barsoukov, J.R. Macdonald, *Impedance Spectroscopy Theory, Experiment, and Applications,* second ed., John Wiley & Sons, Inc., New Jersey, USA, 2005.

[4] M.S. Jayswal, D.K. Kanchan, P. Sharma, M. Pant, *Solid State Ionics* 186 (2011) 7.

[5] A. Sil, R. Sharma, S. Ray, *Surface & Coatings Technology* 271 (2015) 201.

[6] M. Abreha, A.R. Subrahmanyam, J.S. Kumar, *Chemical Physics Letters* 658 (2016) 240.

[7] A.K. Jonscher, J.M. Reau, *J. Mater. Sci.* 1,3 (1978) 563.

[8] P. Sharma, *Ph.D. Thesis*, Department of Physics, The M.S. University of Baroda, Vadodara, 2013.

[9] S.K. Deraman, N.S. Mohamed, R.H.Y. Subban, *Int. J. Electrochem. Sci.* 8 (2013) 1459.

[10] K. Singh, S.S. Bhoga, *Complex Impedance Spectroscopy Solid State Ionics and its Application*, Vol. 1, Ch. 2, 2007, pp.1.

[11] R.A. Senthil, J. Theerthagiri, J. Madhavan, A.K. Arof, *Optical Materials* 58 (2016) 357.

[12] D.F. Vieira, C.O. Avellaneda, A. Pawlicka, *Electrochimica Acta* 53 (2007) 1404.

[13] A.S.A. Khiar, R. Puteh, A.K. Arof, *Physica B* 373 (2006) 23.

[14] S. Summerfield, *Phil. Mag. B* 52 (1985) 9.

[15] B. Roling, A. Happe, K. Funke, M.D. Ingram, *Phys. Rev. Lett.* 78 (1997) 2160.

[16] A. Ghosh, A. Pan, *Phys. Rev. Lett.* 84 (2000) 2188.

[17] J.C. Dyre, P. Maass, B. Roling, D.L. Sidebottom, *Rep. Prog. Phys.* 72 (2009) 046501.

[18] M.S. Jayswal, *Ph.D. Thesis*, Department of Physics, The M.S. University of Baroda, 2014.

[19] M. Pant, *Ph.D. Thesis*, Department of Physics, The M.S. University of Baroda, Vadodara, 2010.

[20] D.L. Sidebottom, *Rev. Mod. Phy.* 81 (2009) 999.

[21] A.K. Jonscher, *Dielectric Relaxation in Solids*, Chelsea Dielectric Press, London, 1983.

[22] P. Joge, D.K. Kanchan, P. Sharma, M. Jayswal, D.K. Avasthi, *Radiation Physics and Chemistry* 100 (2014) 74.

[23] D.K. Mahato, A. Dutta, T.P. Sinha, *Indian Journal of Pure & Applied Physics* 49 (2011) 613.

[24] A.R. Polu, H.W. Rhee, *International Journal of Hydrogen Energy* 42 (2017) 7212.

[25] P. Joge, D.K. Kanchan, P. Sharma, N. Gondaliya, *Advanced Materials Research* 665 (2013) 227.

[26] P. Kesharwani, D.K. Sahu, Y.K. Mahipal, R.C. Agrawal, *Materials Chemistry and Physics* 193 (2017) 524.

[27] N.K. Karan, D.K. Pradhan, R. Thomas, B. Natesan, R.S. Katiyar, *Solid State Ionics,* 179 (2008) 689.

[28] M. Piszcz, H. Zhang, M. Marczewski, G.Z. Zukowska, K. Lemanska, M. Sukiennik, M. Siekierski, *Solid State Ionics* 303 (2017) 78.

[29] P. Pradeepa, S. Edwinraj, M.R. Prabhu, *Chinese Chemical Letters* 26 (2015) 1191.

[30] B. Chatterjee, N. Kulshrestha, P.N. Gupta, *Measurement* 82 (2016) 490.

[31] T. Miyamoto, K. Shibayama, *J. Appl. Phys.* 44 (12) (1973) 5372.

[32] N. Ramesh, J.L. Duda, *J. Membr. Sci.* 191 (1-2) (2001) 13.

[33] S. Rajendran, K. Kesavan, R. Nithya, M. Ulaganathan, *Current Applied Physics* 12 (2012) 789.

[34] G. Choudalakis, A.D. Gotsis, *Current Opinion in Colloid & Interface Science* 17 (2012) 132.

[35] P. Joge, D.K. Kanchan, P. Sharma, N. Gondaliya, *Indian Journal of Pure & Applied Physics* 51 (2013) 350.

[36] M.R. Johan, O.H. Shy, S. Ibrahim, S.M.M. Yassin, T.Y. Hui, *Solid State Ionics* 196 (2011) 41.

[37] P. Joge, D.K. Kanchan, *Advanced Materials Research* 1141 (2016) 19.

[38] P. Joge, D.K. Kanchan, P. Sharma, *Proc. Crystalline and Non-Crystalline Solids*, 2014.

[39] A. Kumar, R. Sharma, M.K. Das, P. Gajbhiye, K.K. Kar, *Electrochimica Acta* 215 (2016) 1.

[40] Q. Wang, W.L. Song, L.Z. Fan, Q. Shi, *Journal of Power Sources* 279 (2015) 405.

[41] P. Sharma, D.K. Kanchan, N. Gondaliya, M. Jayswal, P. Joge, *Indian Journal of Pure & Applied Physics* 51 (2013) 346.

[42] N. Gondaliya, D.K. Kanchan, P. Sharma, P. Joge, *Journal of Applied Polymer Science* 125 (2012) 1513.

[43] K. Vignarooban, M.A.K.L. Dissanayake, I. Albinsson, B.E. Mellander, *Solid State Ionics* 266 (2014) 25.

[44] L. Lee, S.J. Park, S. Kim, *Solid State Ionics* 234 (2013) 19.

[45] R.S. Kumar, K. Hariharan, *Solid State Ionics* 104 (1997) 227.

[46] M. Pant, D. K. Kanchan, P. Sharma, *Ionics* 16 (2010) 797.

[47] D.K. Pradhan, N.K. Karan, R. Thomas, R.S. Katiyar, *Materials Chemistry and Physics* 147 (2014) 1016.

[48] M. Hema, P. Tamilselvi, *Journal of Physics and Chemistry of Solids* 96-97 (2016) 42.

[49] J. Castillo, M. Chacon, R. Castillo, R.A. Vargas, P.R. Beuno, J.A. Varela, *Ionics* 15 (2009) 537.

[50] P. Sharma, D.K. Kanchan, N. Gondaliya, M. Pant, M.S. Jayswal, *Ionics* 19 (2013) 301.

[51] S.B. Aziz, Z.H.Z. Abidin, A.K. Arof, *Express Polymer Letters* 4 (5) (2010) 300.

[52] H. Naili, N. Zouari, T. Mhiri, A. Daoud, *J. Mol. Struct.* 519 (2000) 143.

[53] A.K. Jonscher, *Phys. State Solidi* 32 (1975) 665.

[54] T. Winie, A.K. Arof, *Ionics* 10 (2004) 193.

[55] H.K. Patel, S.W. Martin, *Phys. Rev. B.* 45 (1992) 10292.

[56] R.J. Sengwa, P. Dhatarwal, S. Choudhary, *Electrochimica Acta* 142 (2014) 359.

[57] M. Muthuvinayagam, C. Gopinathan, *Polymer* 68 (2015) 122.

[58] A.K. Nath, A. Kumar, *Electrochimica Acta* 129 (2014) 177.

[59] S.F.M. Zamri, F.A. Latif, A.M.M. Ali, R. Ibrahim, N. Kamaluddin, F. Hadip, *Procedia Technology* 15 (2014) 849.

[60] I.B. Pehlivan, C.G. Granqvist, R. Marsal, P. Georen, G.A. Niklasson, *Solar Energy Materials & Solar Cells* 98 (2012) 465.

[61] B. Jinisha, K.M. Anilkumar, M. Manoj, V.S. Pradeep, S. Jayalekshmi, *Electrochimica Acta* 235 (2017) 210.

[62] R. Blanga, D. Golodnitsky, G. Ardel, K. Freedman, A. Gladkich, Y. Rosenberg, M. Nathan, E. Peled, *Electrochimica Acta* 114 (2013) 325.

[63] N. Angulakhsmi, S. Thomas, J.R. Nair, R. Bongiovanni, C. Gerbaldi, A. Manuel Stephan, *Journal of Power Sources* 228 (2013) 294.

[64] P. Prabakaran, R.P. Manimuthu, *Ionics* 22 (2016) 827.

[65] J.K. Kim, L. Niedzicki. J. Scheers, C.R. Shin, D.H. Lim, W. Wieczorek, P. Johansson, J.H. Ahn, A. Matic, P. Jacobsson, *Journal of Power Sources* 224 (2013) 93.

[66] N. Angulakshmi, D.J. Yoo, K.S. Nahm, C. Gerbaldi, A.M. Stephan, *Ionics* 20 (2014) 151.

[67] R. Prasanth, N. Shubha, H.H. Hng, M. Srinivasan, *Journal of Power Sources* 245 (2014) 283.

[68] X. Yan, B. Peng, B. Hu, Q. Chen, *Polymer* 99 (2016) 44.

[69] P.G. Bruce, C.A. Vincent, *Chem. Soc. Faraday Trans.* 89 (17) (1993) 3187.

[70] S. Raghu, S. Kilarkaje, G. Sanjeev, G.K. Nagaraja, H. Devendrappa, *Radiation Physics & Chemistry* 98 (2014) 124.

[71] M. Kaynak, A. Yusuf, H. Aydin, M.U. Taskiran, A. Bozkurt, *Electrochimica Acta* 164 (2015) 108.

[72] P. Sharma, D.K. Kanchan, N. Gondaliya, *Ionics* 19 (2013) 777.

[73] J.E. Weston, B.C.H. Steele, *Solid State Ionics* 7 (1982) 75.

[74] P. Joge, D.K. Kanchan, P. Sharma, *AIP Conf. Proc.* 1591 (2014) 356.